Molecular Design of Interfacial Layers based on Conjugated Polythiophenes for Polymer and Hybrid Solar Cells

Judith E. Houston[1], Sébastien Richeter[2], Sébastien Clément[2*] and Rachel C. Evans[3,4]*

[1]JülichCentrefor Neutron Science (JCNS) at Heinz Maier-Leibnitz Zentrum (MLZ), Forschungszentrum Jülich GmbH, Lichtenbergstr. 1, 85748 Garching, Germany

[2] Institut Charles Gerhardt – UMR 5253, Université de Montpellier – CC1701, Place Eugène Bataillon, F-34095 Montpellier Cedex 05, France. E-mail: sebastien.clement1@umontpellier.fr; Tel: +33 467143971.

[3]Department of Materials Science & Metallurgy, University of Cambridge, 27 Charles Babbage Road, Cambridge, CB3 0FS, U.K. Email: rce26@cam.ac.uk

[4]School of Chemistry, Trinity College Dublin, Dublin 2, Ireland

ABSTRACT

In the past two decades, bulk heterojunction-organic photovoltaic devices (BHJ-OPVs) have emerged as attractive candidates for solar energy conversion due to their light-weight design and potential for low-cost high-throughput, solution-phase processability. Interfacial engineering is a proven efficient approach to achieve OPVs with high power conversion efficiencies (PCEs). This mini-review provides an overview of the key structural considerations necessary when undertaking the molecular design of conjugated polyelectrolytes (CPEs), for application as interfacial layers (ILs). The different roles of ILs are outlined, together with the advantages and disadvantages of competing classes of IL materials. Particular emphasis is placed on the design and synthesis of water-soluble polythiophene-based IL materials and the influence of their structural characteristics on their performance as a promising class of IL materials. Finally, the challenges and opportunities for polythiophenes as IL materials for OPVs and other solution-processed solar cell technologies (e.g. perovskite solar cells) are discussed.

KEYWORDS:

Organic photovoltaic, polymer solar cell, conjugated polymer, interfacial layer, polythiophene, perovskite

Glossary of acronyms

A	Acceptor
AIL	Anode interfacial layer
BHJ	Bulk heterojunction
CbpNSO	3-((2′-(4″-cyano-biphenyl-4-yloxy)ethyl)-N,N-dimethylammonio)propane-sulfonate
CIL	Cathode interfacial layer
CPE	Conjugated polyelectrolyte
CPZ	Conjugated polymer zwitterion
D	Donor
DFT	Density functional theory
DS	Dodecyl sulfate
EA	Electron affinity
eLbL	Electrostatic Layer by Layer
ETL	Electron transport layer
FF	Fill factor
HOMO	Highest occupied molecular orbital
HTL	Hole transport layer
IE	Ionization energy
IL	Interfacial layer
ILC	Ionic liquid crystal
IQE	Internal quantum efficiency

ITO	Indium tin oxide
J_{sc}	Short-circuit current density
KCTP	Kumada chain transfer polymerisation
KPM	Kelvin probe microscopy
LUMO	Lowest unoccupied molecular orbital
M_n	Number-average molecular weight
NEXAFS	Near edge X-ray absorption fine structure
OPV	Organic photovoltaic
P3AT	Poly(3-alkylthiophene)
P3HT	Poly(3-hexylthiophene)
PBDTT-TT	Poly((4,8-bis(5-(2-ethylhexyl)thiophene-2-yl)benzo[1,2-*b*:4,5-*b'*]dithiophene-2,6-diyl)-*alt*-(2-(((2-ethylhexyl)oxy)carbonyl)-3-fluorothieno[3,4-*b*]thiophenediyl))
PBDTTPD	Poly((4,8-bis((2-ethylhexyl)oxy)benzo[1,2-*b*:4,5-*b'*]dithiophene-2,6-diyl)-*alt*-((N-ethylhexylthieno[3,4-*c*]pyrrole-4,6-dione)-2,6-diyl))
PBDTTT-C-T	Poly((4,8-bis(5-(2-ethylhexyl)thiophene-2-yl)benzo[1,2-*b*:4,5-*b'*]dithiophene-2,6-diyl)-*alt*-(2-(2-ethylhexanoyl)thieno[3,4-*b*]thiophenediyl))
$PC_{61}BM$	Phenyl-C_{61}-butyric acid methyl ester
$PC_{71}BM$	Phenyl-C_{71}-butyric acid methyl ester
PCDTBT	Poly((*N*-9'-heptadecanyl-2,7-carbazole)-*alt*-(5,5-(4',7'-di-2-thienyl-2',1',3'-benzothiadiazole)))
PCDTBT-Pho	Poly[(*N*-9'-(1,17-bis(diethylphosphonate)heptadecanyl)-2,7-carbazole)-*alt*-(5,5-(4',7'-di-2-thienyl-2',1',3'-benzothiadiazole)))

PCE	Power conversion efficiency
PCPDTBT	Poly((2,6-(4,4-bis(2-ethylhexyl)cyclopenta-[2,1-*b*;3,4-*b*′]-dithiophene))-*alt*-(4,7-(2',1',3'-benzothiadiazole)))
PEDOT	Poly(3,4-ethylenedioxythiophene)
PEI	Poly(ethyleneimine)
PFBT	Poly((9,9-dihexylfluorene)-*alt*-(4,7-(2',1',3'-benzothiadiazole)))
PFN	Poly((9,9-bis(3'-(*N,N*-dimethylamino)propyl)-2,7-fluorene)-*alt*-(9,9-dioctyl-2,7-fluorene))
PSC	Perovskite solar cell
PSS	Poly(styrene-sulfonate)
PTB7	Poly((4,8-bis((2-ethylhexyl)oxy)benzo[1,2-*b*:4,5-*b'*]dithiophene-2,6-diyl)-*alt*-(2-(((2-ethylhexyl)oxy)carbonyl)-3-fluorothieno[3,4-*b*]thiophenediyl))
PTB7-Th	Poly((4,8-bis(5-(2-ethylhexyl)thiophene-2-yl)benzo[1,2-*b*:4,5-*b'*]dithiophene-2,6-diyl)-*alt*-(2-(((2-ethylhexyl)oxy)carbonyl)-3-fluorothieno[3,4-*b*]thiophenediyl))
RHC	Rapid heat-cool calorimetry
RMS	Root mean square
SAXS	Small angle X-ray scattering
SDBS	Sodium dodecybenzenesulfonate
TEG	Triethylene glycol
TFSI	Bis(trifluoromethylsulfonyl)imide
TiO_x	Titanium oxide
UPS	Ultraviolet photoelectron spectroscopy

V_{oc}	Open-circuit voltage
W_F	Work function
WO_3	Tungsten oxide
WPF-6-oxy-F	Poly[(9,9-bis(6'-(*N,N,N*-trimethylammonium)hexyl)-2,7-fluorene)-*alt*-(9,9-bis(2'-(2'-(2'-methoxyethoxy)ethoxy)ethyl)-2,7-fluorene)dibromide]
XPS	X-ray photoelectron spectroscopy
ZnO	Zinc oxide

INTRODUCTION

Organic photovoltaic (OPV) devices have emerged as attractive candidates for solar energy harvesting in the urban environment due to their light-weight design and potential for inexpensive manufacturing through solution-based deposition processes.[1-3] The typical device architecture is based on a bulk heterojunction (BHJ) sandwiched between two electrodes, where the BHJ consists of an intimate blend of an electron donor (typically a conjugated polymer) and an electron acceptor (commonly a fullerene derivative). The versatility of synthetic chemistry can be harnessed to tailor the optoelectronic characteristics of the donor and acceptor components and the chemical structures of the most commonly used materials are shown in Scheme 1 (highlighted in bold in the text). To date, power conversion efficiencies (PCEs) of 8-11% have been reported for state-of-the-art single heterojunction cells incorporating phenyl-C_{71}-butyric acid methyl ester (**$PC_{71}BM$**) as the electron acceptor and a low bandgap conjugated polymer such as poly((4,8-bis((2-ethylhexyl)oxy)benzo[1,2-*b*:4,5-*b'*]dithiophene-2,6-diyl)-*alt*-(2-(((2-ethylhexyl)oxy)carbonyl)-3-fluorothieno[3,4-*b*]thiophenediyl)) (**PTB7**)[4]] or its derivative **PTB7-Th** (poly((4,8-bis(5-(2-ethylhexyl)thiophene-2-yl)benzo[1,2-*b*:4,5-*b'*]dithiophene-2,6-diyl)-*alt*-(2-(((2-ethylhexyl)oxy)carbonyl)-3-fluorothieno[3,4-*b*]thiophenediyl)))[5, 6]as electron donors.

However, a simple BHJ structure alone is not sufficient to achieve efficiencies of this magnitude – a more complex multilayer device architecture comprised of interfacial layers on either side of the active donor-acceptor composite is required (Figure 1). These interfacial layers perform a variety of functions, from charge collection and transport,[7,8] to diminishing detrimental factors such as current leakage, poor energy level alignment, charge recombination,*etc*.[9-11]This leads to remarkable improvements in the intrinsic device parameters, such as the short-circuit current density (J_{sc}), open-circuit voltage (V_{oc}) and fill factor (*FF*) and, thus, the overall PCE of the device.

A variety of materials have been investigated as interfacial layer (IL) materials for organic solar cells, including metals (Mg,[12] Ca[13]), metal salts (LiF,[14] Cs_2CO_3[15]), fullerene derivatives[16] and conjugated polyelectrolytes (CPEs).[17-19]Water-soluble CPEs possessing conjugated organic backbones and highly polar charged side chains (*i.e.* containing cationic or anionic groups) are particularly attractive in this regard since their orthogonal solubility prevents re-dissolution of the hydrophobic BHJ layer during device fabrication. Moreover, they are extremely effective as IL materials, and their incorporation can routinely result in a greater than 20% improvement in the PCE compared to reference devices.[18, 20-25] CPEs also offer considerable structural versatility, both in terms of the nature of the repeat unit on the conjugated backbone and the chemical composition of their side-chains.[26]Among the various structural classes, polythiophene-based CPEs have recently emerged as promising new candidates for ILs,[18, 22, 25, 27, 28] as they can be readily synthesized with a high degree of control over their structure and molecular weight, which allows for detailed investigation of structure-property relationships and thus, improved insight into their mode of action as interfacial layers.

In this mini-review, we focus on the key structural considerations when undertaking the molecular design of polythiophene CPEs for application as interfacial layers. Firstly, we consider the primary functions of ILs within the device, which will inform the design strategy. Secondly, we discuss the advantages and disadvantages of competing classes of IL materials, so that potential sources of weakness can be identified and overcome. Informed by this background, we will then present design guidelines for the synthesis of polythiophene CPEs with tailored structures targeted to their application as high performance IL materials. Finally, we finish with a brief outlook into the challenges and opportunities for CPEs as IL materials for OPV and other emerging solar cell technologies.

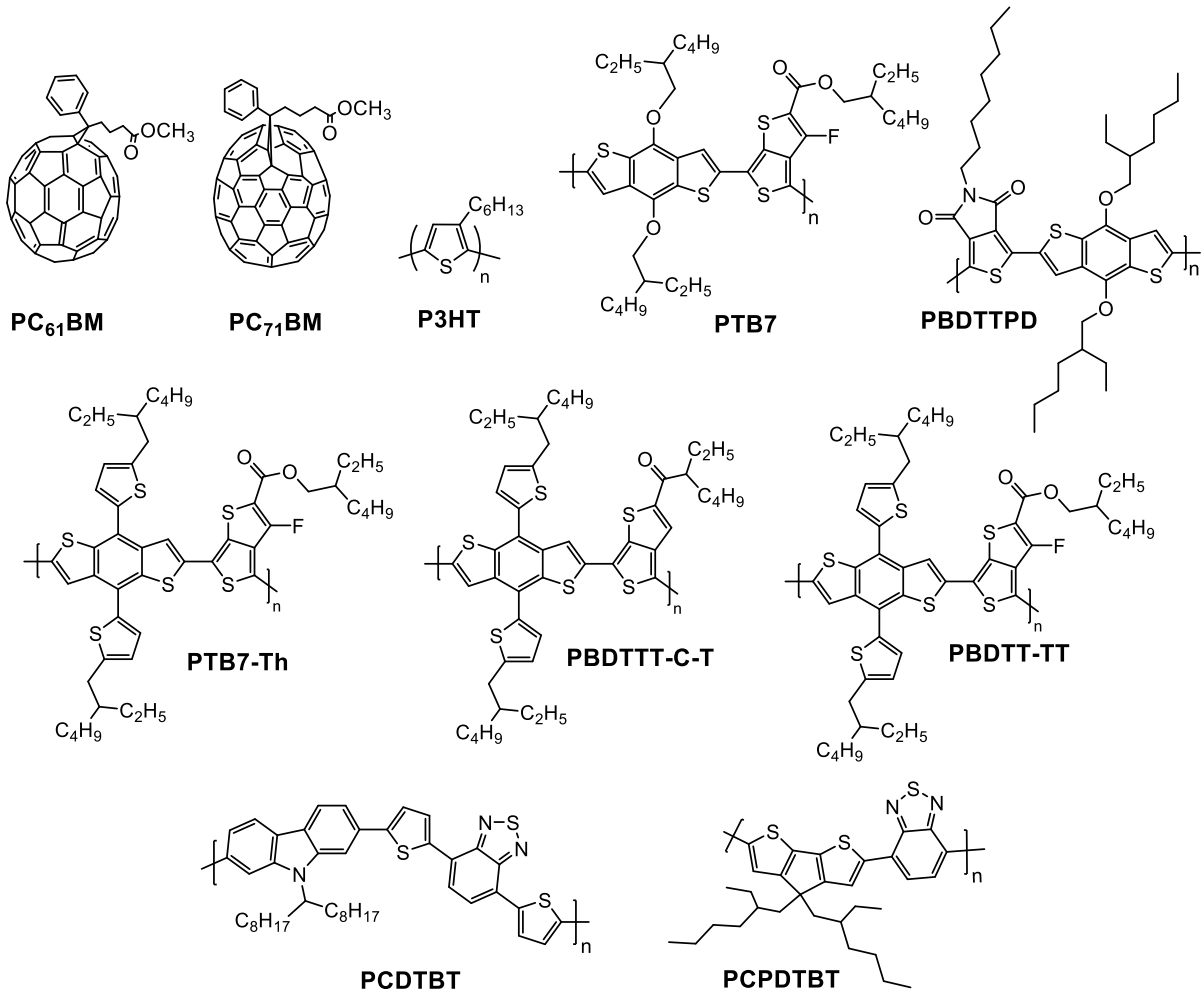

Scheme 1. Chemical structures of electron donor and acceptor materials commonly used in organic photovoltaic devices.

ROLE OF THE INTERFACIAL LAYER

Depending on the direction of charge, OPV cells can be classified as either forward (conventional) or inverted devices, as shown in Figure 1. In the conventional single-junction device, the active and interfacial layers are sandwiched between a transparent anode such as indium tin oxide (ITO) and a low work function (W_F) metal cathode such as Ca or Al. Under solar irradiation, photogenerated excitons in the active layer diffuse towards the donor/acceptor interface where they dissociate into discrete holes and electrons in the highest occupied molecular orbital (HOMO) of the donor and the lowest unoccupied molecular orbital (LUMO) of the acceptor, respectively. From here, the separated holes and electrons

are transported within their respective phases of the active composite until they are collected at the oppositely charged electrodes. In the inverted single-junction device architecture, high W_F metals such as Au or Ag are used as the anode and ITO-modified glass is used as the cathode, which reverses the polarity of charge collection.[4] Since Au and Ag are less air-sensitive than their low W_F metal counterparts, inverted devices are often more stable than conventional OPV cells.[29] In both architectures, anode and cathode interfacial layers (AIL/CIL) are present to mediate charge extraction at the active composite-electrode interfaces, with the ultimate aim of improving the PCE of the device. However, the IL can in fact perform a variety of functions, which are described in more detail below, the nature and extent of which depend on both the material used and the device architecture. The chemical structures of some of the conjugated polymer interlayer materials described (identified as bold in the text) are shown in Schemes 2-5. We note that while some CILs function as electron transport layers (ETLs) and some AILs function as hole transport layers (HTLs), the terms are not synonymous. For clarity, we will only use the terms ETL and HTL if there is clear experimental evidence that the interfacial layer in question contributes directly to the charge transport process.

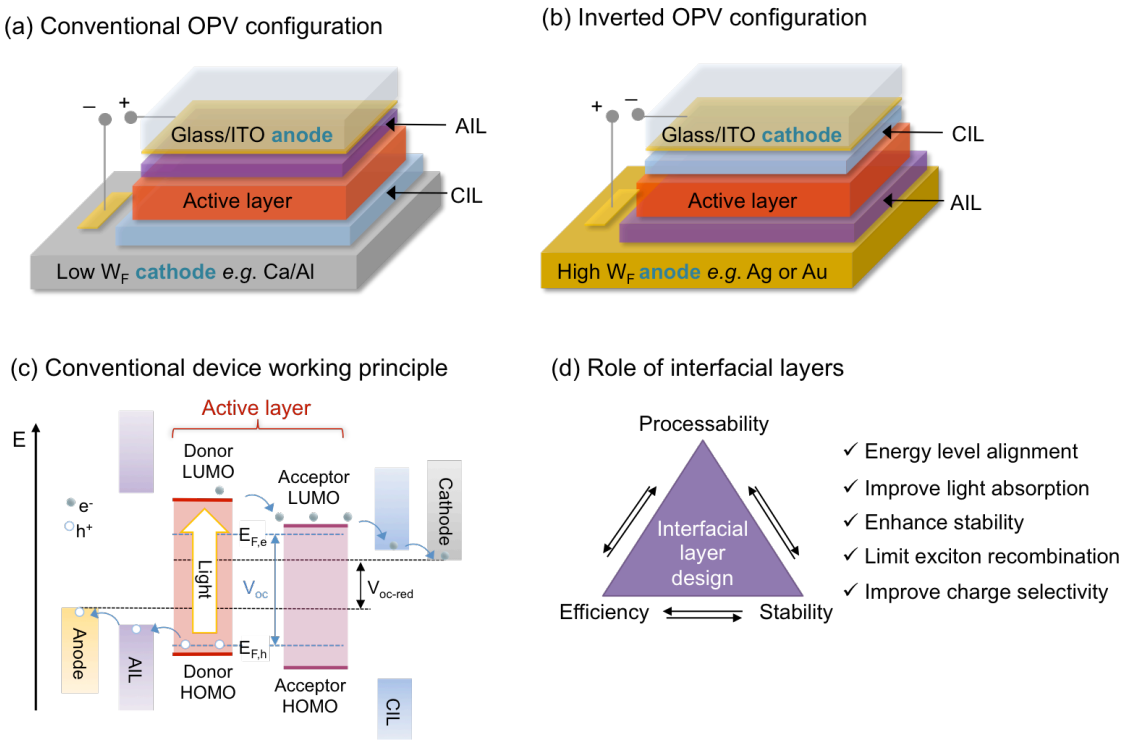

Figure 1. Device architecture and operation of single bulk heterojunction organic photovoltaic (BHJ-OPV) devices. (a) and (b) are schematic representations of conventional (forward) and inverted multilayer device architectures, respectively, where AIL and CIL are the anode and cathode interfacial layers, respectively. (c) Energy level diagram for charge extraction in a conventional OPV device. V_{oc} is the maximum achievable open circuit current and $V_{oc\text{-}red}$ is the reduced V_{oc},which results from non-Ohmic contacts between the active layer materials and the electrodes. (d) Summary of the key functions performed by AIL/CILs in the device.

1. Energy level alignment at the electrode/active layer interface

In BHJ-OPV cells, the maximum achievable V_{oc} is dependent on the difference between the *quasi*-Fermi levels of the photoinduced holes, $E_{F,h}$, formed in the donor and the photoinduced electrons, $E_{F,e}$, generated in the acceptor, and whether Ohmic contacts can be formed with both the electrodes (Figure 1c).[30] When a non-Ohmic *Schottky* contact is formed on either or both sides of the BHJ/electrode interface, the V_{oc} is reduced ($V_{oc\text{-}red}$ in Figure 1c). The magnitude of this reduction will depend on the difference between the work functions of the electrodes.[31]Therefore, it is crucial to understand the interfacial electronic structure and energy level alignment at the electrode/BHJ interface to design better contacts and thus

improve charge extraction. Unfortunately, the nature of contact formation between the electrode and active layer is complicated by a wide variety of interfacial effects including charge transfer, dipole formation, formation of interface states, *etc.,* which depend on the type and strength of interactions between the two materials, as well as the order of contact formation, such as organic-to-metal or metal-to-organic.[32]

The introduction of an interfacial layer can greatly lower the interfacial contact resistance between the hydrophilic metal electrodes and the hydrophobic active BHJ through the formation of interfacial dipoles, which promote Ohmic contact and, thus, improve the V_{oc}(and *FF*).[21, 33]An early study by Heimel *et al.* used density functional theory (DFT) calculations to demonstrate that the orientation of the poly(3-hexylthiophene) (**P3HT**) chains (and also for its fluorinated derivative, where the terminal methyl groups on the hexyl side chains are substituted with $-CF_3$ groups) with respect to the organic/organic or inorganic/organic device interfaces had a decisive impact on energy level alignment at such heterojunctions.[34]In this study, **P3HT** was selected purely as an instructive prototypical material commonly used in organic semiconductor devices. They elucidated that the ionization energies (IE) and the electron affinities (EA) of the polymers were dependent on their orientation. Specifically, the IE and EA of **P3HT** decreased by 0.4 eV between face-on and edge-on configurations, in contrast to fluorinated-**P3HT**, which exhibited an increase of 1.8 eV. The orientation dependence was attributed to the intrinsic surface dipoles of planar π-conjugated systems and the intramolecular polar bonds.[34]Consequently, controlled orientation of polymer chains should dramatically alter the energy level alignment at donor/acceptor or active layer/electrode interfaces within OPV devices. Furthermore, such interfacial dipoles have been shown to increase the surface potential of the active layer, resulting in an increase of the internal built-in potential across the active layer, enabling efficient charge carrier transport and collection.[8] Experimental verification of this function was reported by Oh *et al*.,

who demonstrated that the insertion of water-soluble polyfluorenes, such as poly[(9,9-bis(6'-(*N,N,N*-trimethylammonium)hexyl)-2,7-fluorene)-*alt*-(9,9-bis(2'-(2'-(2'-methoxyethoxy)ethoxy)ethyl)-2,7-fluorene)dibromide] (**WPF-6-oxy-F**), at the interface between a **P3HT**:phenyl-C_{61}-butyric acid methyl ester (**$PC_{61}BM$**) BHJ and a low cost Cu cathode, led to an increase in *FF* and V_{oc}, as well as an enhanced PCE from 0.8% to 3.36%.[24] The polar side groups on the CPE led to the formation of large interfacial dipoles which effectively reduced the W_F of the different metal cathodes investigated (Al, Ag, Cu and Au), leading to Ohmic contact and improved PCEs.[24]

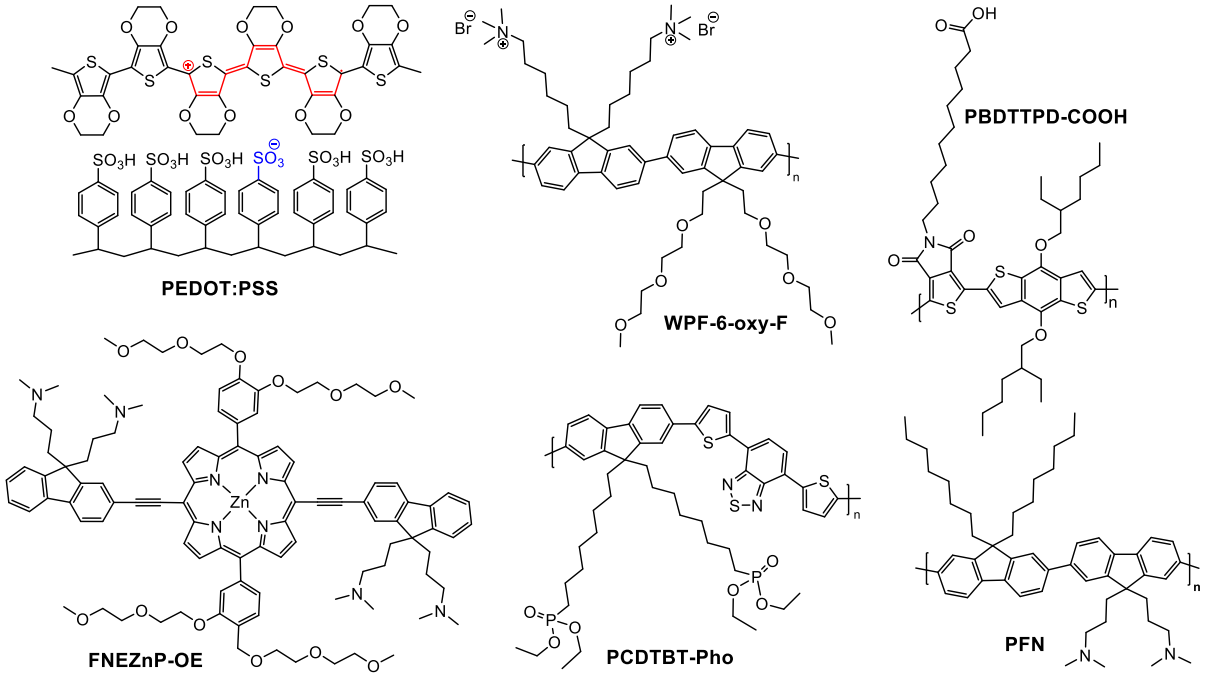

Scheme 2. Chemical structures of some representative conjugated polymers and molecules used as interfacial layer materials in organic photovoltaic devices.

2. Improved charge selectivity and depressed surface/interfacial recombination

In an ideal OPV device, selective contacts on either side of the BHJ composite will collect one charge carrier type, while completely blocking the opposite.[35] However, in a typical homogeneously mixed BHJ layer both the donor and acceptor are in contact with both electrodes. As a direct consequence, undesired charge recombination and electron quenching

can occur at these interfaces. The introduction of interfacial layers can lead to proper charge selectivity at the electrode/active layer interface, thus minimising charge recombination and leading to improved PCE.[13]

As the W_F of an electrode and that of the donor and/or acceptor in the BHJ composite are somewhat mismatched, there is an energy barrier for charge carrier transportation which restricts the charge carrier collection efficiency.[36]Ideally, a HTL or ETL is selected with the appropriate energy alignment with the donor and acceptor, respectively, which can enable barrier-less extraction of electrons and holes to the cathode and anode. Simultaneously, the LUMO of the HTL and HOMO of the ETL should block the flow of electrons and holes to the anode and cathode, respectively. For example, the archetypical anode ITO[32] has a W_F of -4.7 eV,[37]which is significantly higher than that of the HOMO levels (valence bands) of most common organic donor materials (*e.g.***P3HT**, W_F = -5.2 to -4.8 eV[38]). Such a mismatch of energy levels leads to non-Ohmic contact and decreased hole transport. However, if a HTL, such as poly(3,4-ethylenedioxythiophene) (**PEDOT**)/poly(styrene sulfonate) (**PSS**) with a W_F of -5.0 eV,[39] is deposited on top of the ITO electrode, the energy barrier is suppressed and a Fermi contact can be formed.[40] Simultaneously, such HTLs block electron transport and prevent detrimental current leakage,[10]and IL materials with bandgaps larger than those of the donor and acceptor can also help confine excitons in the active layer to increase the probability of exciton dissociation.[41]

3. Controlled surface properties to alter the morphology of the active layer

The effect of interfacial layers on the morphology of the adjacent components should also be considered, since fabrication compatibility is not always guaranteed. When ILs are spin-coated directly on top of a BHJ composite (or *vice versa*), their presence may influence the structural arrangement of the active layer, such as molecular ordering and phase separation, which carries important implications for the operation of BHJ cells.[42] For

example, Karagiannidis *et al.* observed **P3HT** enrichment at the BHJ surface and **$PC_{61}BM$** segregation at the bottom interface when the BHJ was deposited onto more hydrophilic **PEDOT:PSS** substrates.[42] Although this phase separation initially led to improved device efficiency during casting, it introduced significant recombination losses upon annealing.Furthermore, electrodes which have rough surfaces can lead to direct shorts and local high fields and, thus, current leakage can occur.[43]Han *et al.* observed that amorphous tungsten oxide (WO_3) thermally deposited directly on top of an ITO electrode transforms the root mean square (RMS) roughness of the bare ITO surface from 2.80 nm to 0.88 nm, which is comparable to **PEDOT:PSS** modified electrodes (0.81 nm).[44] The observed improvement in *FF* from 0.56 to 0.70, before and after the addition of WO_3, respectively, was attributed to suppressed charge recombination near the anodes due to this reduced surface roughness.

4. Introduction of an optical spacer to modulate light absorption

In both conventional and inverted device architectures incident light enters the OPV cell through the transparent top electrode and is reflected back into the active layer by the metal electrode, forming a standing wave within the device.[4] However, optical interference losses within conventional and inverted devices can result in reduced cell efficiencies.[45,46] Therefore, the ability to control interference effects to maximise the optical field strength within the thin film is important to improve light absorption.[46, 47] By modulating the thickness of transparent ILs, it is possible to enhance photocurrent *via* the *optical spacer* effect.[48] Optical spacer ILs can improve the spatial distribution of light inside the solar cell, and thus, enhance photon absorption within the photoactive layer.[46, 49] Park *et al*. demonstrated a device based on an active BHJ composite of poly((*N*-9'-heptadecanyl-2,7-carbazole)-*alt*-(5,5-(4',7'-di-2-thienyl-2',1',3'-benzothiadiazole))) (**PCDTBT**)/**$PC_{71}BM$**, which had an internal quantum efficiency (IQE) close to 100% upon the addition of a TiO_x optical spacer layer and a PCE of 6%.[48] This remarkable IQE implies that essentially every absorbed photon

results in a separated pair of charge carriers, *i.e.* none of the absorbed photons are lost. Low refractive index metal oxides (n=1.5-1.7[50]), such as TiO_x and ZnO, are better suited as optical spacers as they allow more light to "enter" the BHJ than high refractive index metal oxides such as MoO_3(n=2-2.3).[47]

5. Improved interfacial stability between the active layer and electrodes

ILs can also play an important role in improving device stability.[51-53] This includes the ability to: (i) form robust films to protect the underlying materials from deposition damage of subsequent layers;[32] (ii) create conformal contacts with improved adhesion between the active layer and electrodes which prevent interfacial dewetting and delamination;[52] (iii) hinder the penetration of water and oxygen;[51] and (iv) block the diffusion of unwanted species from the electrodes, such as metal particles, during device fabrication and operation.

CLASSES OF MATERIALS USED IN INTERFACIAL LAYERS

Efficient ILs should encompass a myriad of qualities with respect to their electronic, optical and mechanical properties, including (i) good chemical and physical stability; (ii) solution processability; (iii) excellent film forming properties; (iv) large band gap to confine excitons within the active layer; (v) promote Ohmic contact between the electrodes and the active layer; (vi) appropriate energy levels so as to inject or collect only a single charge carrier type; (vii) low fabrication costs; (viii) zero-absorption of incident radiation and (ix) sufficient conductivity to reduce resistive losses. Clearly, it is challenging to identify a single material that can simultaneously fulfil all these requirements but several classes of materials and their hybrids have been explored. Examples of commonly investigated IL materials, their properties and some disadvantages to be considered, are summarised in Table 1. While the focus of this mini-review is on ILs based on conjugated polythiophenes, it is pertinent to first

discuss competing approaches to glean further insight into the molecular design requirements.

Table 1. Summary of some representative hole-(HTL) and electron-(ETL) transport interfacial layer materials, their properties and disadvantages.

Types of materials	Examples	AIL/ CIL	Properties	Disadvantages
Metals	Mg[12] Ca[13] Ba[54]	CIL	Good conductivity	Air and moisture sensitivity Expensive thermal deposition process
Metal salts	Cs_2CO_3[15] LiF[14, 55]	CIL	Strong interfacial dipole formation Solution processable	Diffusing ions can contaminate the active layer
Transition metal oxides	MoO_3[56] WO_3[44]	AIL	High optical transparency Form smooth uniform layers Good electrode compatibility Eliminates air-sensitive low work function metals	Expensive high vacuum/thermal deposition process
	TiO_x[57] ZnO[49, 58]	CIL	Optical spacer Scalable for large devices	Limited conductivity Require UV light activation
Doped polymers	PEDOT:PSS[59]	AIL/ CIL	Tunable conductivity	Acidic etching of ITO electrodes
Fullerene derivatives	B-PCBO[60]	CIL	Compatibility with organic active layers High conductivity	Expensive materials
Conjugated polyelectrolytes	WPF-6-oxy-F[24] PFN[7]P1,Br[18]	CIL	Solution processable. Strong interfacial dipole formation Tunable electrical properties through structural modification	Performance is sensitive to film thickness
Small molecules	FNEZnP-OE[61]	CIL	Easy purification Tunable electrical properties through structural modification	Performance is sensitive to film thickness Limited conductivity

Low work-function alkali earth metals including Mg (-3.7 eV[62]),[12]Ba (-2.7 eV[62])[54] and Ca (-2.9 eV[62])[13] and alkali metal compounds such as Cs_2CO_3[15] and LiF[14, 55] (W_F<3.0 eV[63]) have been used extensively as the CIL to reduce the W_F of the cathode for more efficient electron extraction. However, these pure metals are air- and moisture-sensitive and can be easily oxidised, which significantly decreases the stability of OPV devices.[64] In addition, the requirement for high vacuum and/or thermal deposition of some metal-based ILs (*e.g.* Cs_2CO_3), may not be compatible with large-scale solution processing techniques.[65] P-type transition metal oxides, such as MoO_x and WO_3, have been investigated as the AIL to enhance the device stability.[63] Although, such materials typically require expensive thermal procedures to be deposited on top of the electrode, Li *et al*. have recently demonstrated a facile route to thin film metal oxide HTLs by spin-coating a methanolic solution of MoO_x on top of the ITO electrode.[56] The resultant films of MoO_x had a smoother surface, better transparency and higher electrical conductivity, leading to an improvement in the PCE from 4.43% (with a PEDOT:PSS AIL) to 4.67% with the MoO_x layer. N-type solution-processed zinc oxide (ZnO)[58, 66]and titanium oxide (TiO_x)[57] have been used as efficient CILs due to their good optical transparency and electron selectivity. These materials are typically used in inverted-OPV devices to improve the electron collection at the cathode. Liang *et al.* showed that the device PCE can be further improved when an electron-rich polymer nanolayer (poly(ethyleneimine) (**PEI**)) is placed on top of a ZnO-based ETL.[58] Devices prepared using only the ZnO or PEI buffer layer show relatively low PCEs of ~7.0% and ~7.5%, respectively. An enhanced PCE of ~8.9% upon dual incorporation was attributed to the lowered conduction band of the ZnO layer, *via* the formation of interfacial dipoles at the interfaces between the ZnO layer and the PEI nanolayer. The PEI nanolayer also improved the surface roughness of the ZnO IL so that the device series resistance noticeably decreased.[58]

Interfacial layer materials that are solution-processable at room temperature thus offer a significant advantage over metal-based ILs. However, as the IL must be deposited on top of, or underneath, the active BHJ composite without damage, orthogonal solubility is a key requirement. The BHJ composite is usually deposited from apolar organic solvents; it is therefore advantageous that the IL material is soluble in water or alcohols. Small molecule analogues of chlorophylls, porphyrins and their derivatives have been intensively investigated as IL materials due to their large π-conjugated planes and easy chemical modifications of the peripheries to improve the intramolecular charge transport and electron transfer.[61, 67, 68] For example, Zhang *et al.* developed a CIL based on a water-soluble conjugated porphyrin, **FNEZnP-OE**, in which two amino-functionalized fluorenes are linked to a porphyrin core by ethylene linkages.[61] A conventional device incorporating the CIL and based on a**PTB7-Th**:**$PC_{71}BM$** active layer exhibited a PCE of 9.16%, which was a 41% increase compared to the device with no CIL (6.5%).[61] The improvement was attributed to a decrease in the W_F of the cathode through the surface dipole interaction of the amino-functionalised polar side groups, with the extended π-conjugated backbone of **FNEZnP-OE** by the ethynyl linkages thought to be beneficial for enhanced electron transport.

The archetypical organic HTL materials are based on doped polymers, most commonly **PEDOT:PSS**, which is typically used to modify the ITO anodes and assist hole extraction from the active layers, due to its high electron conductivity, transparency in the visible region of the spectrum and resistance to the organic solvents used for subsequent layer deposition.[59] In addition, **PEDOT:PSS** simultaneously smooths rough ITO surfaces leading to a reduction in losses due to charge recombination.[69]However, the electron-blocking capability of **PEDOT:PSS** is not optimal, and it has even been incorporated as an electron acceptor in inverted-OPV devices.[70] Moreover, the acidic nature of **PEDOT:PSS** in a conventional device architecture is known to etch ITO and cause OPV degradation.[71] An

alternative approach is to further modify the **PEDOT:PSS** by the addition of a thin polymer overlayer between the electrode and the BHJ composite.[72] However, this extra layer is known to complicate matters, such as energy level alignment and the local morphology of the BHJ.[9, 72] For example, Cao *et al*. incorporated a low-bandgappolymer, based upon poly((4,8-bis((2-ethylhexyl)oxy)benzo[1,2-*b*:4,5-*b'*]dithiophene-2,6-diyl)-*alt*-((N-ethylhexylthieno[3,4-*c*]pyrrole-4,6-dione)-2,6-diyl)) (**PBDTTPD**) with a carboxylic acid-based side chain, **PBDTTPD-COOH**, as an interfacial modifier between the ITO/**PEDOT:PSS** and BHJ layers in an OPV device in order to deconvolute the possible role of such overlayers in the organisation of the active layer.[9] They concluded that the observed improvement in PCE upon addition of the overlayer in their devices was primarily driven by changes in the BHJ composition at the anode.[9] It was found that after addition of the **PBDTTPD-COOH** layer, the buried interface was no longer PCBM-rich, which reduced the extent of charge recombination at the interface and improved the PCE.[9] Meng *et al.* found that an overlayer of poly[(*N*-9'-(1,17-bis(diethylphosphonate)heptadecanyl)-2,7-carbazole)-*alt*-(5,5-(4',7'-di-2-thienyl-2',1',3'-benzothiadiazole))) (**PCDTBT-Pho**) on top of **PEDOT:PSS** caused the subsequently deposited BHJ composite layer of **PCDTBT:PCBM** to form a bicontinuous network, rather than the more homogenous morphology of the reference device.[72] This architecture led to improved charge separation and transport, an increase in J_{SC} by 12% and PCE enhancement of 8% for the OPV device.

Water-soluble conjugated polyfluorene electrolytes have been investigated widely as CIL materials.[20, 24, 73-75] Poly((9,9-bis(3'-(*N,N*-dimethylamino)propyl)-2,7-fluorene)-*alt*-(9,9-dioctyl-2,7-fluorene)) (**PFN**) is potentially the CPE most commonly used as a cathodic interlayer.[7] For example, Sun *et al.* observed an enhancement in PCE, from 6.13% to 7.72%, upon incorporation of a **PFN** cathodic IL between an active layer of **PTB7-Th:PC_{71}BM** and an Al electrode.[7]The improvement was attributed to the strong interfacial dipoles formed by

the thin **PFN** layer, which caused an enhancement in the built-in potential across the active layer, and led to efficient charge carrier transport and collection.[7] Furthermore, it was shown that an even greater enhancement of 12.6% could be achieved if the active layer was first pre-soaked in a methanol solution, which was attributed to more ideal vertical phase separation.[7] Chen *et al.* found that increasing the number of polar groups in polyfluorene-based ETLs improved the coverage of favourable interfacial dipoles on the surface of ITO in an inverted OPV device. Dipole formation led to an enhancement in the electrostatic interaction between the active layer and the electrode, thus minimizing the interfacial energy barrier.[20] Since the ordering and orientation of the polymer controls the orientation of the dipole moment,[21] detailed understanding of the structural organisation of organic interlayers with respect to their charge transport properties is therefore crucial to further optimise the performance of OPV devices.

Recently, water-soluble polythiophenes, in particular, poly(3-alkylthiophenes) (**P3ATs**) have emerged as a promising class of IL materials. The main advantage of the polythiophene backbone lies in the ready availability of convenient synthetic strategies, *e.g.* Kumada Catalyst-Transfer Polycondensation (KCTP),[76] which not only enable the relatively straightforward preparation of polythiophenes with multiple topographies (homopolymers, random/block copolymers) and a high degree of control over the final structure and molecular weight, but also facilitate tuning of the optical and self-assembly properties of polythiophene-based IL materials. Although these IL materials present a powerful approach in view of improving the OPV characteristics, clear guidelines with respect to their structure are required for designing high-performance polythiophene-based IL materials. In this regard, we will discuss below the influence of the polythiophene structural characteristics (nature of the ionic side group, topology, molecular weight…) on their performance as interfacial layers.

MOLECULAR DESIGN AND PERFORMANCE OF POLYTHIOPHENE IL MATERIALS

1.Nature of the ionic pendant group

In 2011, Bazan *et al.* reported on polythiophene-type cathodic interfacial materials containing pendant trimethylammonium groups (**P1,Br**) (Scheme 3).[18] For conventional architecture OPVcells based on **PCDTBT:PC$_{71}$BM**, a PCE of 6.1% was obtained using a ETL based on this CPE, compared to 5.0% in its absence (Entry 1, Table 2). The ionic ammonium pendant groups allow orthogonal processing on top of the photoactive layer and grant the formation of a capacitive double layer, enabling improved charge extraction and thus, device efficiency.[22] When **P1,Br** was used as the CIL in **P3HT:PC$_{61}$BM**-based OPVs annealed in air, the PCE was enhanced from 1.80% to 2.57% (Entry 2, Table 2).[27] In this case, the chain interactions between the **P3HT** donor and the **P1,Br** ETL enhanced the contact between the active layer and the Al electrode, resulting in improved electron extraction efficiency, as well as reduced electron-hole recombination. Replacing the ionic ammonium moieties with another ionic group may have a beneficial effect on the inherent I-V properties of OPVs. The use of imidazolium-substituted polythiophenes (**P2,Br**) (Scheme 3) as a CIL in standard architecture **PCDTBT:PC$_{71}$BM** solar cells resulted in a PCE of 6.22%, a clear enhancement in comparison to the reference device (5.23%) and also, devices with **P1,Br** or **PFN** as the interfacial layer (6.03%) (Entry 3, Table 2).[17] **P2,Br** was also found to be suitable as an ultrathin interlayer cathode in inverted organic solar cells.[77] Indeed, the deposition of the ionic polythiophene thin layer (less than 10 nm) decreased the W_F of the ITO (4.4 eV *vs*. 4.8 eV for neat ITO), enabling similar performances to TiO_x interlayers to be attained, when combined with either a **PCDTBT:PC$_{71}$BM** or **P3HT:PC$_{61}$BM** (Entry 4, Table 2) photoactive layer. However, UV exposure (commonly

found in ITO/metal oxide (TiO_x or ZnO) interfaces and known as "light-soaking") is required to achieve a high FF on the order of 60%, as well as a reduced W_F on the ITO.[78]

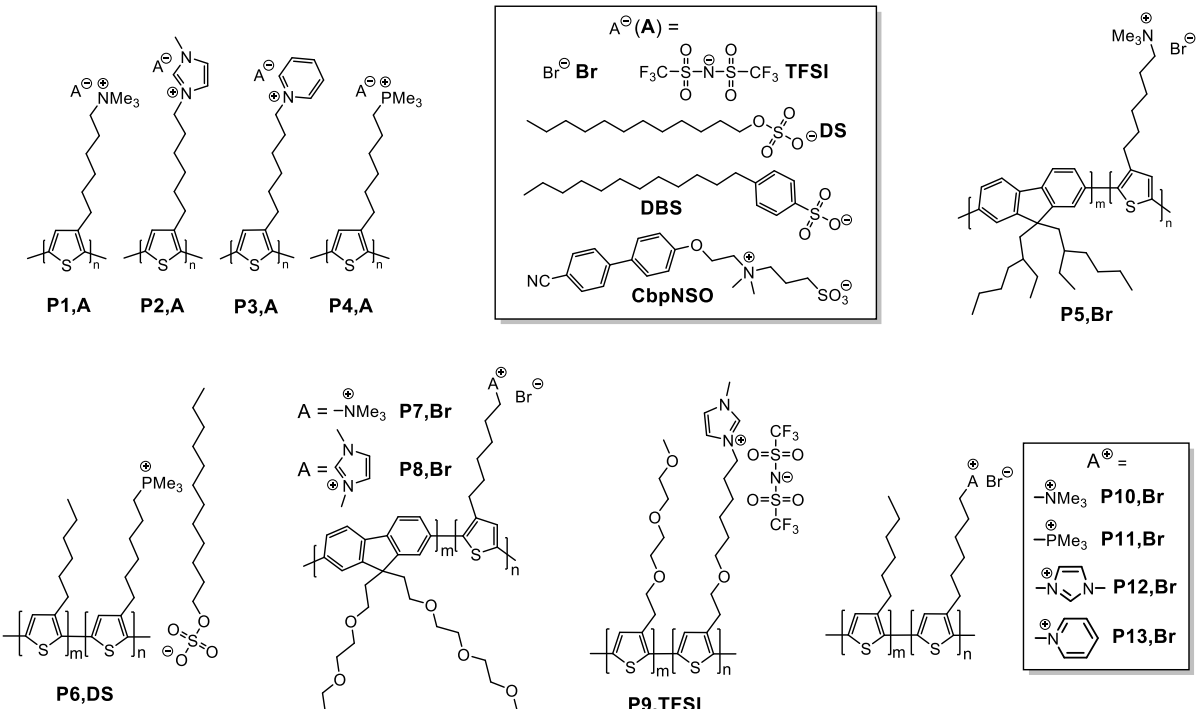

Scheme 3. Chemical structures of some polythiophene-based interfacial layer materials for organic photovoltaic devices.

More recently, Maes *et al.* examined a broader array of ionic polythiophenes (**P2-P4,TFSI**) (Scheme 3) aiming to establish clear structural guidelines for the design of efficient polythiophene-based ILs.[22] Pyridinium (**P3,TFSI**) and phosphonium (**P4,TFSI**)-substituted polythiophenes outperformed their imidazolium counterparts leading to PCEs of 7.90% for **P3,TFSI** and 7.72% for **P4,TFSI** *vs*. 7.44% for **P2,TFSI** when combined with **PBDTTPD:$PC_{71}BM$** as the photoactive layer (Entry 5, Table 2). Although the surface coverage on top of the photoactive layer was found to be comparable in these examples (Figure 2),[17,22] the observed morphology of the IL was noticeably different. In general, these materials lead to an incomplete photoactive layer coverage with the formation of stain-like structures with highly different height-width ratios depending on the ionic pendant

groups.[17,18,22] As such, a high affinity of the CPE with respect to the underlying photoactive layer is required to achieve the highest performance enhancement in the OPV device.

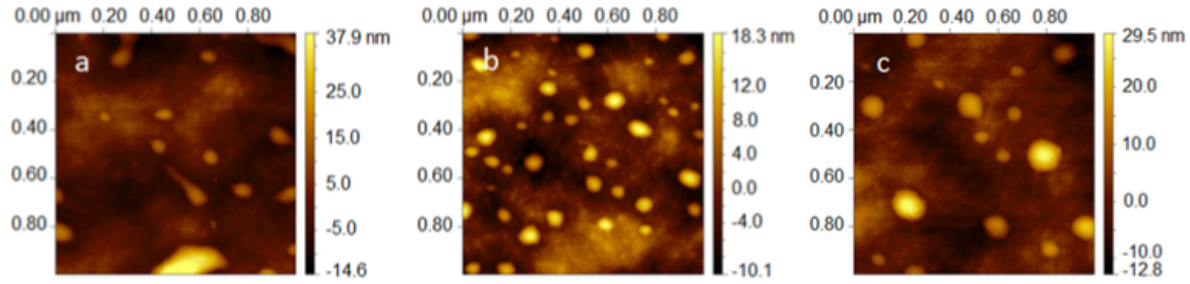

Figure 2. AFM topography images of a **PBDTTPD**:**PC$_{71}$BM** photoactive layer coated with(a) **P2,TFSI**, (b) **P3,TFSI** and(c) **P4,TFSI** interfacial layers. The relative surface area coverage for the IL is 12, 19 and 13 for **P2–P4,TFSI**, respectively. Adapted with permission from Ref. [22] Copyright 2016 American Chemical Society.

2.Molecular weight

The polymer chain length has also been identified as an important parameter controlling the IL performance. Maes *et al.* reported two ionic imidazolium-functionalized polythiophene homopolymers (**P2,Br**) with varying molecular weight (M_n = 11.2 kDa and 32.6 kDa, respectively, for the bromide precursor polymers) for application as CILs in conventional OPV cells.[17] When used in combination with **PCDTBT:PC$_{71}$BM** as the photoactive layer, the best PCE of 6.22% was obtained for the highest molecular weight polymer (Entry 3, Table 2).

3. Topology of the polymer

Charge extraction and transfer are intimately linked to the morphology of the IL. As such, control of the morphology is crucial, especially in inverted solar cells, where the morphology of the photoactive layer and thus, the device performance can be severely affected by the cathode interfacial topology.[79] In this respect, block copolymers are an interesting route to control the self-assembly of the IL material into nanostructured morphologies, which is driven by the thermodynamic incompatibility of the two blocks.[80,81] Scherf *et al.* have notably shown that amphiphilic conjugated block copolymers containing

both hydrophobic polyfluorene and hydrophilic cationic poly(3-hexylthiophene) blocks (**P5,Br**) (Scheme 3) exhibit solvent- and charge-mediated self-assembly.[80, 82-84] Judicious selection of the solvent mixture polarity allows modulation of the nanomorphology of the self-assembled aggregates (*e.g.* vesicles, rods, *etc.*), as well as their optical properties.[72, 82-85] Due to its solubility in polar solvents, this conjugated block copolyelectrolyte was used as an electron-extracting layer in BHJ-OPV cells and its performance was compared to that of the corresponding ionic polythiophene homopolymer (**P1,Br**).[18] The CPE block showed a moderately improved performance compared to its homopolymer counterpart, leading to PCEs of 6.2% and 6.1%, respectively, when combined with **PCDTBT:$PC_{71}BM$** as the photoactive layer (Entry 1, Table 2). Water contact angle (θ) measurements performed on the surface of **PCDTBT:$PC_{71}BM$** and **PCDTBT:$PC_{71}BM$**/CPE layers indicated that compared to the hydrophobic photoactive layer ($\theta \approx 90°$), introduction of the CPE IL leads to a moderately hydrophilic surface for **P1,Br** ($\theta \approx 45°$) and fully hydrophilic surface for **P5,Br** ($\theta < 30°$), which suggests accumulation of the ionic component at the topmost organic surface (Figure 3).

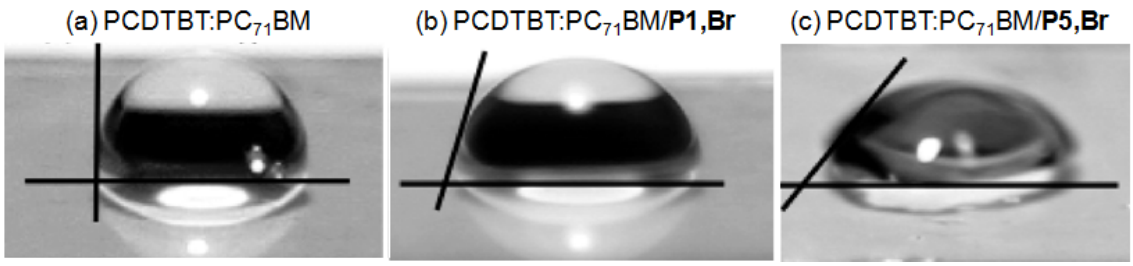

Figure 3. Photographs of water droplets on the surfaces of (a) **PCDTBT:$PC_{71}BM$**, **PCDTBT:$PC_{71}BM$** after spin-casting of (b) 0.01% **P1,Br**, and (c) 0.02% **P5,Br** on **PCDTBT:$PC_{71}BM$** substrates. Adapted with permission from ref.[18] Copyright 2011 American Chemical Society.

The segregation of the hydrophobic and hydrophilic blocks in **P5,Br** provides a more polar surface, which may lead to improved formation of interfacial dipoles and may explain the slightly better PCE. A similar positive effect in solar cell performance was also observed

for CILs based on all-conjugated cationic diblock copolymers composed of two polythiophene blocks (**P6,DS**) with regard to their homopolyelectrolyte counterpart (**P4,DS**) (Scheme 3).[25] When combined with a **PBDTTPD:PC$_{71}$BM** photoactive layer, CILs based on both the homo and diblock CPEs led to an PCE improvement of >20% compared to the corresponding device incorporating a Ca interfacial layer, mainly due to an increase in the J_{sc} (Entry 7, Table 2). **P4,DS** and **P6,DS** exhibit similar photovoltaic performance leading to PCEs of 8.65% and 8.78%, while **P6,DS** shows a higher affinity towards deposition on top of the photoactive layer. This indicates that while the affinity of the IL material for the photoactive layer is important for obtaining optimal photovoltaic performance, additional parameters such as the permittivity of the CPEs and the ability to create a stable capacitive double layer are also required.[22]

Recently, Chen *et al.* investigated the influence of the intrinsic self-assembly of diblock CPEs as CILs on the arrangement and morphology of the upper active layer in inverted organic solar cells.[79] The two water/alcohol-soluble diblock CPEs with ammonium (**P7,Br**) and imidazolium (**P8,Br**) ionic groups (Scheme 3) substantially reduced the work function of ITO *via* modulation of the interfacial dipoles:W_F = 4.56eV for **P7,Br** and W_F = 4.24 eV for **P8,Br** *vs.*W_F = 4.85 eV for pure ITO, as determined by ultraviolet photoelectron spectroscopy (UPS). The differences in the W_F of the two diblock-CPE modified electrodes were found to depend on the polar nature of the terminal ionic group on the side chains, with imidazolium derivatives leading to a larger dipole moment than quaternary ammonium salts, as evidenced by Kelvin probe microscopy (KPM) and DFT calculations. These diblock CPEs spontaneously self-assemble into a scolopendra-like face-on arrangement on the ITO cathode and act as a template to induce partial face-on arrangement of the donor. This face-on orientation of the donor results in improved charge mobility along the π–π stacking direction relative to that along the lamellar direction and overall an increased PCE.[86] Hence, using

P7,Br and **P8,Br** as CILs with a **P3HT:$PC_{61}BM$** photoactive layer, the device PCE was improved from 0.8% to 3.1% and 3.5%, respectively (Entry 8, Table 2).[79]

The density of the ionic functionality in CPEs is an important parameter to consider in view of fine-tuning their electrical properties.[87] In addition, although the presence of ionic pendant groups allows the creation of a capacitive double layer, which improves charge extraction and thus, device efficiency, it reduces affinity of the IL material for the hydrophobic photoactive layer.[22] In this respect, Maes *et al.* prepared a specific random (50/50) copolythiophene with triethylene glycol and imidazolium-substituted hexyloxyethyl side chains (**P9,TFSI**)[88] (Scheme 3) and used it as a CIL in an OPV device.[22, 89]Compared to traditional alkyl side chains as previously used in the copolymers mentioned above, triethylene glycol (TEG) side chains allow a high polarity and solubility in polar solvents to be maintained. For conventional OPV cells based on **PBDTTPD:$PC_{71}BM$**, a PCE of 8.21% was obtained using this CPE as the IL, compared to 7.44% for the imidazolium-based homopolyelectrolyte (**P2,TFSI**) (Entry 5, Table 2). By introducing a certain amount of non-ionic side chains, the affinity of the material to the photoactive layer was enhanced compared to its homopolyelectrolyte counterpart. Impedance spectroscopy measurements performed on **P3,TFSI** and **P9,TFSI** materials also indicated that the presence of the TEG chains in the random copolymer stabilize the interfacial dipole.

4. Nature of the counterion

Charge-compensating counterions should be taken into consideration in the molecular design of CPEs since their properties (size, hydrophobicity, mobility, redox potential, charge density...) enable fine-tuning of the optoelectronic properties both in solution and in the solid-state.[90-93]Bazan *et al.* have notably reported that the solid-state photoluminescence properties of a cationic CPE based on a poly((9,9-dihexylfluorene)-*alt*-(4,7-(2',1',3'-benzothiadiazole))) backbone (**PFTB-X**) (Scheme 4) can be manipulated by changing the size of counterion:

larger anions lead to increased interchain distance and thereby, increased emission quantum yields.[94] The same authors also showed that replacing the bromide counterion with the larger *tetrakis*(1-imidazolyl)borate (BIm_4^-) anion in a cationic narrow bandgap CPE (Scheme 4) derived from poly((2,6-(4,4-bis(2-ethylhexyl)cyclopenta-[2,1-*b*;3,4-*b*']-dithiophene))-*alt*-(4,7-(2',1',3'-benzothiadiazole))) (**PCPDTBT**) framework (Scheme 3) not only modified the HOMO and LUMO energy levels, but also, its semiconducting character (*p*-type for Br^- and *n*-type for BIm_4^-).[92]

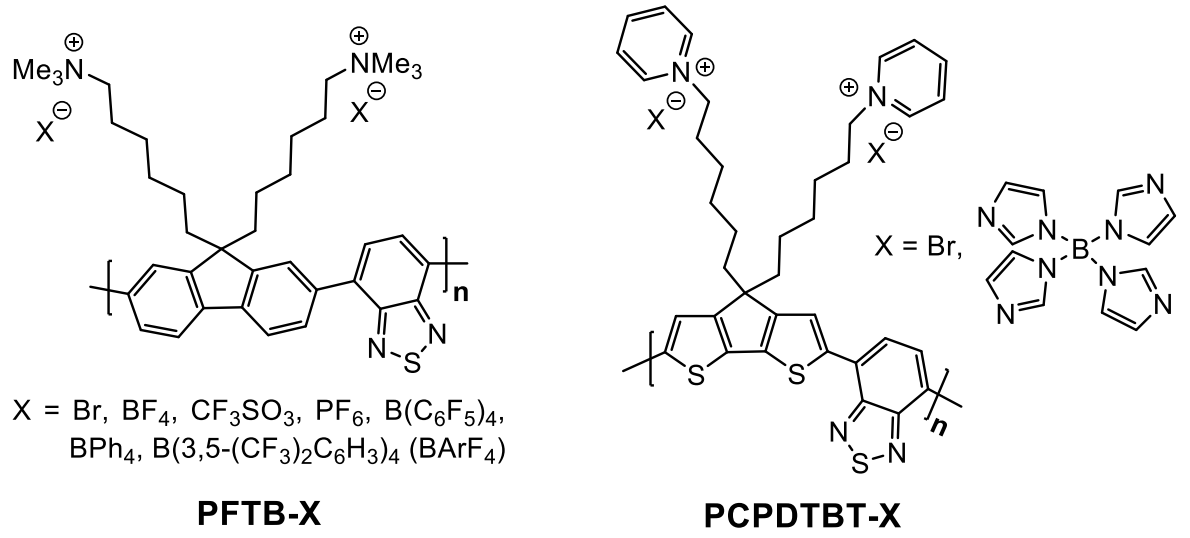

Scheme 4. Structure of **PFTB-X** and **PCPDTBT-X** based CPEs containing various anionic counterions.

Generally, ionic side groups are introduced by quaternization of a bromide-bearing precursor polymer, thus leading to CPEs with a bromide counterion. The presence of this bromide counterion implies that all these CPEs exhibit a strong hygroscopic behaviour.[22, 88, 95] Indeed, rapid heat-cool calorimetry (RHC) analysis of both cationic homopolyelectrolytes (**P2-P4,Br**) and block copolyelectrolyte-based **P3HT** CPEs (**P10-P13,Br**) (Scheme 3) revealed an important endothermic effect during the first heating, which indicated the presence of a significant amount of water. During the second heating cycle, this effect is no longer present but reappears when these materials are stored under ambient conditions, proving their hydrophilicity.[95] Since the performance of CPEs as interfacial layers involves

the formation of dipoles at the interface, the presence of a variable amount of water in these CPEs may lead to a high irreproducibility in the device efficiency. For these reasons, hygroscopic bromide anions should be avoided and exchanged for more hydrophobic counterions such as bis(trifluoromethylsulfonyl)imide (**TFSI**).[22]

By judiciously choosing the nature of the counterion, the ordering and orientation of the polymer and hence, the orientation of the dipole moment can be controlled. In 2012, Yang *et al.* reported the electrostatic self-assembly of an ammonium-substituted polythiophene (**P1,Br**) with the anionic surfactant, sodium dodecybenzenesulfonate (**SDBS**) (Scheme 3).[21] The stoichiometric CPE:surfactant complex exhibited very high stability (over a couple of weeks) against humidity compared to **P1,Br** alone or **P1:DBS** complexes with non-stoichiometric ratios (2:1 and 1:2). The presence of the **DBS** counterion results in more ordered packing of the polymer backbone in **P1,DBS**, as illustrated by its red-shifted absorption (~20 nm) in films with respect to **P1,Br**. This cathodic interlayer material not only performs well with the hydrophobic **P3HT:PC$_{61}$BM** photoactive layer (PCE = 4.01% for **P1,DBS** *vs*. 3.81% with a Ca IL)[21] but also, with low bandgap polymer-based BHJ systems such as **PTB7:PC$_{71}$BM** (PCE = 6.47% for **P1,DBS** *vs.* 5.46% with a Ca IL) (Entry 9, Table 2). A similarly beneficial effect on device performance was also observed when dodecyl sulfate (DS) surfactant was used as a counterion to replace bromide.[25] When **P4,DS** was used as a CIL in conventional OPV devices based on **PBDTTPD:PC$_{71}$BM**, the PCE was enhanced from 7.18% to 8.65% (Entry 7, Table 2). Beyond the improvement in device efficiency, enhanced device stability in air may be also achieved by using such CPE-surfactant complexes as ILs instead of Ca.[21]

By exploiting the electrostatic self-assembly between an ionic liquid crystal (ILC), namely 3-((2′-(4″-cyano-biphenyl-4-yloxy)ethyl)-*N,N*-dimethylammonio)propanesulfonate (**CbpNSO**) and **P1,Br**, the interfacial dipole orientation and thus, the W_F of ITO (4.02 eV for

P1,CbpNSO *vs.* 4.93 eV for neat ITO) was also manipulated in inverted OPV cells.[96] Indeed, introduction of ILC pendant groups led to improved ordering of the CPE and thus, crystallinity in the film, as observed by small angle X-ray scattering (SAXS), which is more desirable for forming an aligned dipole moment.[97] The reduction in W_F caused by the enhanced orientation of dipole moment also increases the built-in field, which helps to facilitate exciton dissociation and increase the photogenerated-carrier collection. For instance, inverted OPV devices based on **P3HT** and the low bandgap poly((4,8-bis(5-(2-ethylhexyl)thiophene-2-yl)benzo[1,2-*b*:4,5-*b'*]dithiophene-2,6-diyl)-*alt*-(2-(2-ethylhexanoyl)thieno[3,4-*b*]thiophenediyl)) (**PBDTTT-C-T**) with the **P1:CbpNSO** complex (Scheme 3) exhibit an improvement of the average device efficiency when compared with a ZnO ETL (Entry 10, Table 2).[96] In addition, due to the strong ability of liquid crystals to orient themselves along the direction of the field,[98, 99] the dipole orientation in the **P1:CbpNSO** interlayer can be readily manipulated by applying an external electric field.

5. Zwitterionic polythiophenes

Although the CPEs described above improve the performance of OPV cells when incorporated as ILs, the presence of a mobile counterion which migrates during device operation and redistributes the internal electric field,[100-102] can affect the long-term photovoltaic performance. In this respect, conjugated polymer zwitterions (CPZs) with cations and anions covalently bonded together to eliminate mobile ions have been developed as interfacial layers in OPVs.[103] In 2013, Emrick *et al.* reported the synthesis of sulfobetaine-substituted polythiophene CPZs with methylene (**P14**) and butylene tethers (**P15**) separating the zwitterions from the backbone (Scheme 5).[104] Due to the electron-withdrawing effect of the cationic group on the zwitterion,[103] the length of the CH_2 spacer was found to dramatically influence the ionization potential and band gap of these polymers, going from 2.19 eV for **P14** to 1.96 eV for **P15**.[104] The influence of the alkyl spacer is also reflected in

the photovoltaic performance obtained for **P14** and **P15**. Both **P14** and **P15** improved the efficiency of OPVs when used as an IL in combination with **PTB7:PC$_{71}$BM**, with the highest values being obtained for longer side chains.[105] Since the improvement of the device performances are correlated with the value and the orientation of the interfacial dipole, the greater side chain flexibility for **P15** is believed to facilitate their orientation along the surface. Near edge X-ray absorption fine-structure (NEXAFS) measurements indicated a face-on orientation for CPZs with respect to the underlying active layer.[105] Moreover, modelling of the electrostatic alignment of the dipolar zwitterionic side chains in the vicinity of a metal surface revealed that the anion of the zwitterion points towards the surface, leading to a negative interfacial dipole. This interfacial dipole can be further improved by replacing a thiophene unit by benzothiadiazole (**P16** and **P17**, Scheme 5), leading to higher device performance (2.82% for **P16** and 5.85% for **P17**; interlayer thickness: 5 nm).[105] The HOMO and LUMO levels, and the band gap, of polythiophene-based CPZs can be adjusted by incorporating acceptor moieties such as diketopyrrolopyrrole or isoindigo units, thus enabling their electron-extracting and hole-blocking capabilities to be modulated.[106] For example, compared to pure polythiophene-based CPZs, CPZs containing isoindigo backbones (**P18-20**) exhibit deeper HOMO levels and lower band gaps (Scheme 5). As such, the energy levels of these isoindigo-based polythiophene CPZs ($E_{HOMO} \approx$ -4.09 eV, $E_{LUMO} \approx$ -5.67 eV) are well-positioned with respect to the HOMO of **PTB7** (E_{HOMO} = -3.63 eV) and LUMO level of **PC$_{71}$BM** (E_{LUMO} = -5.87 eV) allowing efficient electron-extraction and hole-blocking. Thus, these CPZs were found to significantly improve the OPV performance in comparison with a control device, with a PCE in the range of 7.28%-7.73% obtained for isoindigo-based CPZs *vs.* 1.55% for control device.[106]

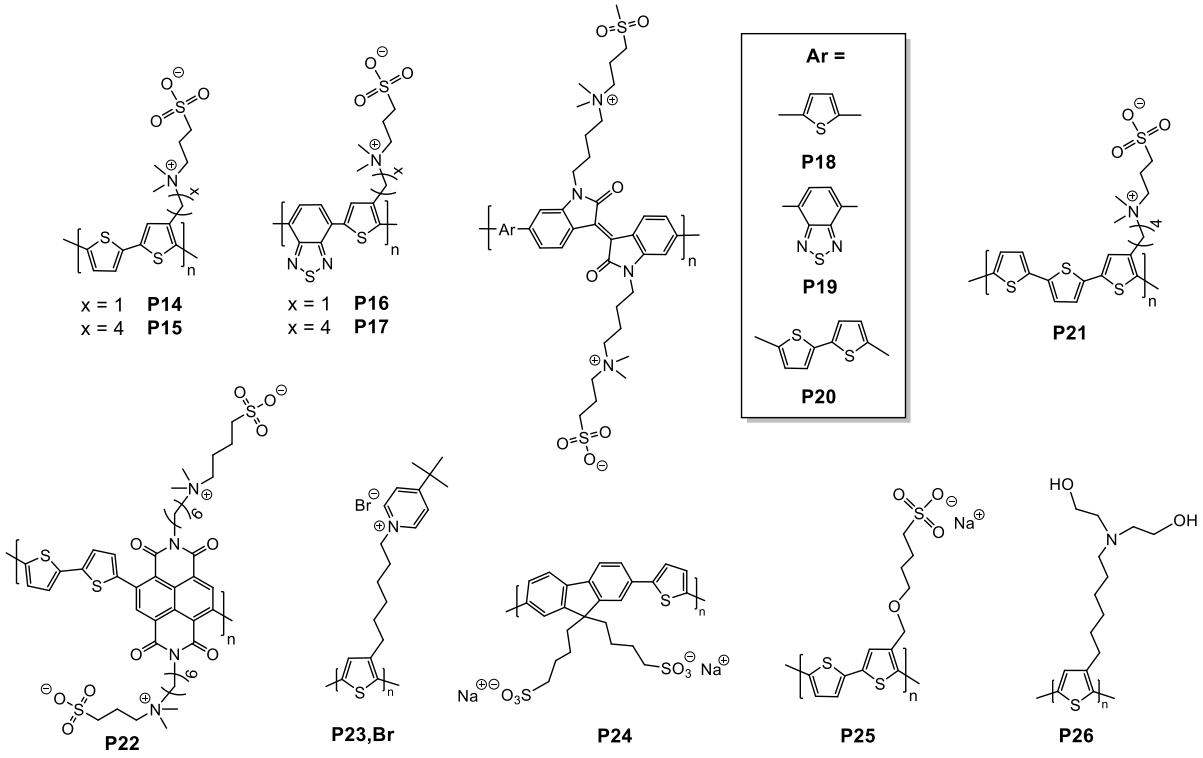

Scheme 5. Chemical structures of polythiophene-based interfacial layer materials for organic photovoltaic devices including conjugated polymer zwitterions (CPZs).

The nature of the conjugated backbone in CPZs is also important since it influences the electron-transport properties of the interfacial layer. Indeed, due to their p-type character, polythiophene-based CPZs are not overly favourable for electron transport, and their performance declines rapidly with the layer thickness.[103] For example, for devices containing a **P21** interlayer, a dramatic decrease in both the J_{sc} and *FF* was obtained when the thickness was increase up to 7 nm, leading to a poor PCE (< 1%). To overcome this problem, Emrick *et al.* reported polythiophene CPZs-type cathodic interfacial materials containing a naphthalenediimide backbone (**P22**) (Scheme 5).[107] These CPZs were found to be less sensitive to variations in the layer thickness, since high PCEs (6.95%) could be reached even with a significant layer thickness (> 20 nm). For standard architecture OPV cells based on poly((4,8-bis(5-(2-ethylhexyl)thiophene-2-yl)benzo[1,2-*b*:4,5-*b'*]dithiophene-2,6-diyl)-*alt*-(2-(((2-ethylhexyl)oxy)carbonyl)-3-fluorothieno[3,4-*b*]thiophenediyl)) (**PBDTT-TT)**:**PC$_{71}$BM**,

a PCE of 9.99% was obtained with **P22** as the IL, compared to 3.17% without interlayer and 5.02% with a **P21** interlayer (Entry 11, Table 2).[107]

6. Co-assembly of polythiophene-based CPEs with PEDOT:PSS

As described above, **PEDOT:PSS** is an ubiquitous material in OPV devices, which is usually used as an anodic IL on ITO to improve the electrode roughness, the Ohmic contact with the photoactive layer, hole collection and to increase V_{oc}.[108] Unfortunately, due to its electron-blocking properties, **PEDOT:PSS** is generally not used as an interlayer in inverted polymer solar cells. In addition, it also affects the lifetime of OPVs since (i) its acidic nature can promote ITO etching[109] and (ii) the excess of PSS can migrate in the photoactive layer and react with its components.[110] To circumvent this, Buriak *et al.* combined water-soluble cationic pyridinium-substituted polythiophenes (**P3,Br** and **P23,Br**) with anionic **PEDOT:PSS** on ITO through an electrostatic layer-by-layer (eLbL) assembly.[28, 111] By successively immersing an ITO substrate into an aqueous solution of either the cationic polythiophene or **PEDOT:PSS**, (**P3**/**PEDOT:PSS**)$_n$ and (**P23**/**PEDOT:PSS**)$_n$ multilayer films with thicknesses depending on the number of bilayers (*n*) were prepared (Figure 4).

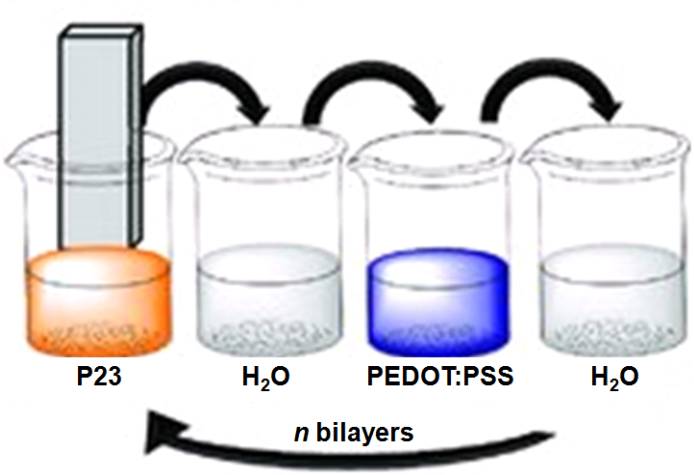

Figure 4. Fabrication of a**P23**/**PEDOT:PSS** bilayer on an ITO substrate by electrostatic layer-by-layer (eLbL). Adapted with permission from ref.[111]Copyright 2012 WILEY-VCH Verlag GmbH & Co. KGaA, Weinheim.

Upon introduction of these pyridinium-substituted polythiophenes, the W_F of the ITO was found to decrease from 4.6 eV to 3.8 eV beyond $n = 3$.[111] It is interesting to note that up to $n = 3$, the W_F of the ITO oscillates predictably between approximately 3.8 and 4.0 eV irrespective of the repeated cycles. This behaviour was assigned to the modulation of the electron affinity of ITO.[112] The appropriate value of the W_F of the ITO/(**P23**/**PEDOT:PSS**)$_{5.5}$ multilayer enabled its use as a cathodic interfacial modifier for inverted polymer solar cells incorporating a photoactive layer composed of either **P3HT**:**PC$_{61}$BM** or **PBDTTPD**:**PC$_{71}$BM**. Devices fabricated using this IL material exhibit PCEs of 3.8% and 5.6% for **P3HT** and **PBDTTPD** donor polymers, respectively.[111] In addition to these good efficiencies, significant long-term stability in air was demonstrated for both devices, with **P3HT**:**PC$_{61}$BM** and **PBDTTPD**:**PC$_{71}$BM** devices maintaining 83% of the initial performance after one year of storage and 97% of the initial performance after 1000 h of storage in air, respectively (Entry 12, Table 2).

The drawbacks associated with the acidity and hygroscopicity of **PEDOT:PSS** may be offset through the introduction of additives. In this respect, the anionic CPE poly[9,9-bis(4-sulfonatobutyl)fluorene-*alt*-thiophene] (**P24**) (Scheme 5) was added to **PEDOT:PSS** solutions in various concentrations.[113] **P24** acts as a conjugate base against the –SO_3H of PSS, allowing the acidity of the HTL to be decreased. Removal of the sodium ions in **P24** results in the formation of a molecular dipole between the –SO_3^- pendant group and the backbone which can screen the coulombic attraction between **PEDOT** and **PSS**.[114, 115] By tuning the amount of **P24** in the **PEDOT:PSS**, the surface potential and conductivity of the HTL could be improved. As a result, when 0.4 wt% of **P24** was added to a **PEDOT:PSS** solution, a maximum PCE of 8.2% *vs.* 7.8% for pristine **PEDOT:PSS** was reached in a conventional OPV architecture based on the **PTB7**:**PC$_{71}$BM** system (Entry 13, Table 2).[113]

More importantly, the long-term stability of these devices was also increased by more than five times compared to the pure **PEDOT:PSS** HTL.

7. Co-assembly of polythiophene CPEs with metal oxides

A remarkable improvement in device performance can be achieved by the incorporation of CPEs with *n*-type metal oxides into polymer solar cells as the ETL.[79, 116] This combination can provide improved band alignment at the **PCBM**-cathode interface and better contact between the active layer and metal oxide, thus improving the PCE.[117, 118] Chen *et al.* reported the synthesis of three polythiophenes bearing anionic sulfonate (**P25**), neutral diethanolamino (**P26**) (Scheme 5) and cationic ammonium (**P1,Br**) groups (Scheme 3).[116] These polymers were deposited on the surface of ZnO to form a ZnO/CPE ETL in inverted polymer solar cells with the goal of determining how the nature of the charge on the CPE influences the interfacial interaction and how it can improve the device performance. Under these conditions, the nitrogen atom of **P26** is partially protonated, as evidenced by X-ray photoelectron spectroscopy (XPS). In the case of ZnO/**P1,Br** and ZnO/**P26** ETLs, XPS measurements also indicated a shift to lower binding energy for the O_2^- ions which may be associated with the higher negative charge density due to the electrostatic interaction operating between the CPE and ZnO. Electrostatic interactions at the ZnO−CPE interface promoted orientation of the polar groups and backbone of CPE leading to the formation of an interfacial dipole between CPE and ZnO layer. This electrostatic self-assembly also allows voids at the ZnO−active layer interface to be filled, and thus improved alignment of the LUMO energy, as well as compatible interactions at the ZnO−active layer interface. Consequently, smoother films (with the exception of **P25**) and a more hydrophobic surface were achieved when depositing these CPEs onto ZnO films.[116] The anionic polythiophene **P25** provides the lowest device performance (3.47%) due to the lack of electrostatic interactions and a built-in potential, which induces a positive dipole orientation (Entry 14,

Table 2). When partially protonated, amine (**P26**) and ammonium (**P1,Br**)-substituted polythiophenes were used in combination with ZnO, higher PCEs of 3.98% and 4.08%, respectively, due to the strong electrostatic interactions were reached (Entry 14, Table 2). It is also important to note that UV treatment for ZnO/cationic **P1,Br** ETL enabled further improvement of the PCE to 4.45% (Entry 14, Table 2).

Block copolyelectrolytes can also be used as ETLs in combination with ZnO. Chen *et al.* deposited polyfluorene-polythiophene-based diblock copolyelectrolytes (**P7,Br** and **P8,Br**) (Scheme 3) on ZnO to form a bilayer ETL in inverted polymer solar cells fabricated from a blend of the low bandgap polymer **PTB7-Th** and **$PC_{71}BM$**.[79] By combining these block copolyelectrolytes with ZnO, the PCE was significantly boosted from 8.1% for bare ZnO to 8.9% and 9.2% for ZnO/**P7,Br** and ZnO/**P8,Br**, respectively (Entry 15, Table 2). These improved efficiencies were ascribed to the simultaneous increase of *FF* and J_{sc}. Indeed, compared to devices with pristine ZnO, ZnO/**P7,Br** and ZnO/**P8,Br**-based devices exhibit enhanced electron mobilities from 1.392×10^{-3} to 4.930×10^{-3} and 5.241×10^{-3} cm^2 V^{-1} s^{-1}, respectively.

Table 2. Summary of key device parameters for representative organic photovoltaic devices incorporating water-soluble polythiophene interlayer (IL) materials extracted from the literature.

Entry	Device Architecture	IL	V_{OC} [a] (V)	J_{SC} [b] (mAcm^{-2})	FF [c]	PCE [d] (%)	Ref.
1	ITO/PEDOT:PSS/PCDTBT:$PC_{71}BM$/IL/Al		0.82	9.7	0.61	5.0	18
		P1,Br	0.86	10.8	0.66	6.1	
		P5,Br	0.89	10.6	0.67	6.2	
2	ITO/PEDOT:PSS/ P3HT:$PC_{61}BM$/IL/Al		0.46	8.93	0.44	1.80	27
		P1,Br	0.59	10.67	0.41	2.57	
3	ITO/PEDOT:PSS/PCDTBT:$PC_{71}BM$/IL/Al		0.73	11.36	0.41	3.39	17
		P1,Br (32.6 kDa)	0.88	11.82	0.58	6.03	
		P2,Br (11.2 kDa)	0.84	11.67	0.55	5.32	
		P2,Br (32.6 kDa)	0.87	12.05	0.59	6.22	
		PFN	0.88	11.84	0.58	5.96	
4	ITO/IL/PCDTBT:$PC_{71}BM$/MoO_3/Ag		0.66	9.8	0.31	2.0	77
		TiO_x	0.85	10.2	0.56	4.9	
		P2,Br	0.84	11.2	0.51	4.8	
	ITO/IL/ P3HT:$PC_{61}BM$/MoO_3/Ag		0.35	8.5	0.29	0.9	
		TiO_x	0.54	10.5	0.60	3.4	
		P2,Br	0.53	10.4	0.61	3.3	
5	ITO/PEDOT:PSS/PBDTTPD:$PC_{71}BM$/IL/Al	**Ca**	0.92	11.28	0.71	7.32	22
		P2,TFSI	0.92	11.57	0.70	7.44	
		P3,TFSI	0.93	12.12	0.70	7.90	
		P4,TFSI	0.92	11.73	0.71	7.72	
		P9,TFSI	0.93	12.25	0.72	8.21	
6	ITO/PEDOT:PSS/PCDTBT:$PC_{71}BM$/IL/Al	**Ca**	0.85	10.15	0.53	4.54	22
		P9,TFSI	0.89	11.55	0.59	6.01	
7	ITO/PEDOT:PSS/ PBDTTPD:$PC_{71}BM$/IL/Al	**Ca**	0.93	11.32	0.69	7.18	25
		P4,DS	0.93	13.20	0.70	8.65	
		P6,DS	0.93	13.52	0.70	8.78	
8	ITO/IL/P3HT:$PC_{61}BM$/MoO_3/Ag		0.38	6.09	0.33	0.8	79
		P7,Br	0.59	8.74	0.58	3.1	
		P8,Br	0.60	8.92	0.65	3.5	
9	ITO/PEDOT:PSS/ P3HT:$PC_{61}BM$/IL/Al	**Ca**	0.60	9.14	0.55	3.81	21

		P1,DBS	0.62	9.54	0.68	4.01	
	ITO/PEDOT:PSS/ PTB7:$PC_{71}BM$/IL/Al	**Ca**	0.72	11.9	0.64	5.46	
		P1,DBS	0.77	12.3	0.68	6.47	
10	Glass/ITO/IL/P3HT:$PC_{61}BM$/PEDOT:PSS/Ag		0.34	9.64	0.32	1.04	96
		ZnO	0.58	10.1	0.56	3.29	
		P1,CbpNSO	0.57	11.7	0.60	4.00	
	Glass/ITO/IL/PBDTTT-C-T:$PC_{71}BM$/MoO_3/Ag	**ZnO**	0.77	14.3	0.60	6.61	
		P1,CbpNSO	0.77	16.4	0.59	7.41	
11	ITO/PEDOT:PSS/PTB7:$PC_{71}BM$/IL/Al	**P21**	0.55	17.94	0.52	5.08	107
		P22	0.76	18.91	0.70	9.99	
12	Glass/ITO/IL/P3HT:$PC_{61}BM$/V_2O_5/Al	**(P23:PEDOT:PSS)$_{5.5}$**	0.55	9.9	0.60	3.8	111
	Glass/ITO/IL/PBDTPD:$PC_{71}BM$/MoO_3/Ag	**(P23:PEDOT:PSS)$_{5.5}$**	0.91	11.2	0.55	5.6	
13	ITO/IL/PTB7:$PC_{71}BM$/PFN/Al	**PEDOT:PSS**	0.76	14.1	72.8	7.8	113
		P24(0.4wt%)/ PEDOT:PSS	0.77	14.9	71.3	8.2	
14	ITO/ZnO/IL/P3HT:$PC_{61}BM$/PEDOT:PSS/Ag		0.57	10.5	0.50	2.99	116
		P1,Br	0.59	12	0.57	4.08	
		P25	0.59	11.3	0.52	3.47	
		P26	0.60	11.9	0.56	3.98	
	ITO/ZnO/IL/P3HT:$PC_{61}BM$/PEDOT:PSS/Ag (UV treatment 20 min)	**P1,Br**	0.61	11.9	0.61	4.45	
15	ITO/ZnO/IL/PTB7-Th:$PC_{71}BM$/MoO_3/Ag		0.77	16.46	0.63	8.1	79
		P7,Br	0.77	17.28	0.67	8.9	
		P8,Br	0.77	17.44	0.68	9.2	

[a] Open-circuit voltage [b] Short-circuit current [c] Fill factor [d] Power conversion efficiency

SUMMARY AND OUTLOOK

CPEs are frequently used as interfacial, charge transport and extraction layer materials in OPVs. Among the CPEs exploited as interfacial layers, ionic polythiophenes have emerged as highly attractive candidates due to their environmental/thermal stability, electrical conductivity and solution processability. In addition, the availability of robust synthetic methods offers the opportunity to prepare multiple polymer topographies (homopolymers, random/block copolymers) with a high degree of control over the final structure and molecular weight. However, although ILs based on polythiophene CPEs have been shown to significantly improve the device performance, much more work lies ahead to establish clear guidelines with respect to their chemical structure. Indeed, numerous design parameters can be envisaged for polythiophene-based CPEs including the nature of the ionic pendant groups and counterions, the molecular weight and the topology. As discussed in this mini-review, such structural features significantly affect the morphology (chain packing, molecular orientation, crystallinity), their affinity for the photoactive layer, their electronic properties and finally, the overall device performance. Even though some design rules have already been formulated, further efforts on polythiophene-based copolyelectrolytes regarding their monomer composition are in particular required. Indeed, by finely tuning the nature of the monomer incorporated in these CPEs and their composition, their electronic properties (mobility, band gap…) as well as their interaction with the metal and the photoactive layer can be controlled to optimize the OPV performance.

Although this mini-review has focussed on the role of polythiophene CPEs as interfacial layers in polymer solar cells, much of the insight gleaned from this review of the recent literature is also applicable to other solution-processed photovoltaic devices, and in particular perovskite solar cells (PSCs). Although still in their infancy, PSCs have been catapulted into the spotlight due to their extremely high reported power-conversion efficiencies (>20%

certified[119]) obtained over a very short research period. Similar to the field of organic photovoltaics, initial attention has concentrated on engineering the architecture of the photoactive perovskite layer.[120, 121] However, as this has become better understood, the focus has begun to shift towards the roles of interfacial layers, since the challenges of energy level alignment, charge extraction and passivation of trap sites are also common to PSCs.[122] While **PEDOT:PSS** remains the most commonly investigated polymeric HTL, more recently various *p*-type conjugated polymers (*e.g.* **PCDTBT, P3HT, PCPDTBT**) have also been incorporated as AILs in p-i-n PSCs and were found to reduce the W_F of ITO/**PEDOT:PSS**, thereby reducing the potential barrier at the interface with the photoactive layer.[123] Similarly, the introduction of a thin layer of **P1,Br** between an ETL of $\mathbf{PC_{61}BM}$ and the Ag cathode led to a decrease in the W_F of Ag from 4.7 eV to 4.13 eV due to the formation of interfacial dipoles with a negative charge.[124] Although there are only a handful of reports in the literature thus far demonstrating the use of polythiophenes, and indeed conjugated polymers in general, as interfacial layers in PSCs, this is certain to change as the field matures and benefits from the lessons learned by the organic photovoltaics community.

ACKNOWLEDGEMENTS

SC and SR thank the CNRS and the Université de Montpellier for financial support. Support from COST action MP1202 and the Ireland-France ‘‘Hubert Curien Ulysses’’ programme (grant no. 31998ZF) is gratefully acknowledged.

References

1 M. Kaltenbrunner, M. S. White, E. D. Głowacki, T. Sekitani, T. Someya, N. S. Sariciftci and S. Bauer, *Nature Communications* **3:**770 (2012).
2 K. Wang, C. Liu, T. Meng, C. Yi and X. Gong, *Chemical Society Reviews* **45:**2937-2975 (2016).
3 K. A. Mazzio and C. K. Luscombe, *Chemical Society Reviews* **44:**78-90 (2015).
4 Z. He, C. Zhong, S. Su, M. Xu, H. Wu and Y. Cao, *Nature Photonics* **6:**591-595 (2012).
5 Z. He, B. Xiao, F. Liu, H. Wu, Y. Yang, S. Xiao, C. Wang, T. P. Russell and Y. Cao, *Nature Photonics* **9:**174-179 (2015).
6 Q. Wan, X. Guo, Z. Wang, W. Li, B. Guo, W. Ma, M. Zhang and Y. Li, *Advanced Functional Materials* **26:**6635-6640 (2016).

7 Q. Sun, F. Zhang, J. Wang, Q. An, C. Zhao, L. Li, F. Teng and B. Hu, *Journal of Materials Chemistry A* **3:**18432-18441 (2015).
8 H. Ma, H. L. Yip, F. Huang and A. K. Y. Jen, *Advanced Functional Materials* **20:**1371-1388 (2010).
9 B. Cao, X. He, C. R. Fetterly, B. C. Olsen, E. J. Luber and J. M. Buriak, *ACS Applied Materials & Interfaces* **8:**18238-18248 (2016).
10 A. W. Hains, J. Liu, A. B. F. Martinson, M. D. Irwin and T. J. Marks, *Advanced Functional Materials* **20:**595-606 (2010).
11 H.-L. Yip and A. K. Y. Jen, *Energy & Environmental Science* **5:**5994-6011 (2012).
12 M. O. Reese, M. S. White, G. Rumbles, D. S. Ginley and S. E. Shaheen, *Applied Physics Letters* **92:**053307 (2008).
13 H. Ju, K. M. Knesting, W. Zhang, X. Pan, C.-H. Wang, Y.-W. Yang, D. S. Ginger and J. Zhu, *ACS Applied Materials & Interfaces* **8:**2125-2131 (2016).
14 M. Gao, J. Subbiah, P. B. Geraghty, M. Chen, B. Purushothaman, X. Chen, T. Qin, D. Vak, F. H. Scholes, S. E. Watkins, M. Skidmore, G. J. Wilson, A. B. Holmes, D. J. Jones and W. W. H. Wong, *Chemistry of Materials* **28:**3481-3487 (2016).
15 G. Li, C.-W. Chu, V. Shrotriya, J. Huang and Y. Yang, *Applied Physics Letters* **88:**253503 (2006).
16 C.-Z. Li, C.-C. Chueh, H.-L. Yip, K. M. O'Malley, W.-C. Chen and A. K. Y. Jen, *Journal of Materials Chemistry* **22:**8574-8578 (2012).
17 J. Kesters, T. Ghoos, H. Penxten, J. Drijkoningen, T. Vangerven, D. M. Lyons, B. Verreet, T. Aernouts, L. Lutsen, D. Vanderzande, J. Manca and W. Maes, *Advanced Energy Materials* **3:**1180-1185 (2013).
18 J. H. Seo, A. Gutacker, Y. Sun, H. Wu, F. Huang, Y. Cao, U. Scherf, A. J. Heeger and G. C. Bazan, *Journal of the American Chemical Society* **133:**8416-8419 (2011).
19 Z. Sun, K. Xiao, J. K. Keum, X. Yu, K. Hong, J. Browning, I. N. Ivanov, J. Chen, J. Alonzo, D. Li, B. G. Sumpter, E. A. Payzant, C. M. Rouleau and D. B. Geohegan, *Advanced Materials* **23:**5529-5535 (2011).
20 H. Liu, L. Hu, F. Wu, L. Chen and Y. Chen, *ACS Applied Materials & Interfaces* **8:**9821-9828 (2016).
21 Y.-M. Chang, R. Zhu, E. Richard, C.-C. Chen, G. Li and Y. Yang, *Advanced Functional Materials* **22:**3284-3289 (2012).
22 J. Kesters, S. Govaerts, G. Pirotte, J. Drijkoningen, M. Chevrier, N. Van den Brande, X. Liu, M. Fahlman, B. Van Mele, L. Lutsen, D. Vanderzande, J. Manca, S. Clément, E. Von Hauff and W. Maes, *ACS Applied Materials & Interfaces* **8:**6309-6314 (2016).
23 T. Yamamoto, D. Komarudin, M. Arai, B.-L. Lee, H. Suganuma, N. Asakawa, Y. Inoue, K. Kubota, S. Sasaki, T. Fukuda and H. Matsuda, *Journal of the American Chemical Society* **120:**2047-2058 (1998).
24 S.-H. Oh, S.-I. Na, J. Jo, B. Lim, D. Vak and D.-Y. Kim, *Advanced Functional Materials* **20:**1977-1983 (2010).
25 M. Chevrier, J. E. Houston, J. Kesters, N. Van den Brande, A. E. Terry, S. Richeter, A. Mehdi, O. Coulembier, P. Dubois, R. Lazzaroni, B. Van Mele, W. Maes, R. C. Evans and S. Clement, *Journal of Materials Chemistry A* **3:**23905-23916 (2015).
26 H. Jiang, P. Taranekar, J. R. Reynolds and K. S. Schanze, *Angewandte Chemie International Edition* **48:**4300-4316 (2009).
27 K. Yao, L. Chen, Y. Chen, F. Li and P. Wang, *Journal of Materials Chemistry* **21:**13780-13784 (2011).
28 D. A. Rider, B. J. Worfolk, K. D. Harris, A. Lalany, K. Shahbazi, M. D. Fleischauer, M. J. Brett and J. M. Buriak, *Advanced Functional Materials* **20:**2404-2415 (2010).
29 B. H. Lee, I. H. Jung, H. Y. Woo, H. K. Shim, G. Kim and K. Lee, *Advanced Functional Materials* **24:**1100-1108 (2014).
30 C. J. Brabec, A. Cravino, D. Meissner, N. S. Sariciftci, T. Fromherz, M. T. Rispens, L. Sanchez and J. C. Hummelen, *Advanced Functional Materials* **11:**374-380 (2001).
31 V. D. Mihailetchi, P. W. M. Blom, J. C. Hummelen and M. T. Rispens, *Journal of Applied Physics* **94:**6849-6854 (2003).

32 H. Ishii, K. Sugiyama, E. Ito and K. Seki, *Advanced Materials* **11:**605-625 (1999).
33 H. Choi, J. S. Park, E. Jeong, G.-H. Kim, B. R. Lee, S. O. Kim, M. H. Song, H. Y. Woo and J. Y. Kim, *Advanced Materials* **23:**2759-2763 (2011).
34 G. Heimel, I. Salzmann, S. Duhm, J. P. Rabe and N. Koch, *Advanced Functional Materials* **19:**3874-3879 (2009).
35 B. Xiao, H. Wu and Y. Cao, *Materials Today* **18:**385-394 (2015).
36 S. Khodabakhsh, B. M. Sanderson, J. Nelson and T. S. Jones, *Advanced Functional Materials* **16:**95-100 (2006).
37 J. S. Kim, J. H. Park, J. H. Lee, J. Jo, D.-Y. Kim and K. Cho, *Applied Physics Letters* **91:**112111 (2007).
38 M. Baghgar and M. D. Barnes, *ACS Nano* **9:**7105-7112 (2015).
39 A. M. Nardes, M. Kemerink, M. M. de Kok, E. Vinken, K. Maturova and R. A. J. Janssen, *Organic Electronics* **9:**727-734 (2008).
40 R. Şahingöz, H. Kanbur, M. Voigt and C. Soykan, *Synthetic Metals* **158:**727-731 (2008).
41 P. Peumans and S. R. Forrest, *Applied Physics Letters* **79:**126-128 (2001).
42 P. G. Karagiannidis, N. Kalfagiannis, D. Georgiou, A. Laskarakis, N. A. Hastas, C. Pitsalidis and S. Logothetidis, *Journal of Materials Chemistry* **22:**14624-14632 (2012).
43 G. Liu, J. B. Kerr and S. Johnson, *Synthetic Metals* **144:**1-6 (2004).
44 S. Han, W. S. Shin, M. Seo, D. Gupta, S.-J. Moon and S. Yoo, *Organic Electronics* **10:**791-797 (2009).
45 K. S. Nalwa and S. Chaudhary, *Optics Express* **18:**5168-5178 (2010).
46 A. K. K. Kyaw, D. H. Wang, D. Wynands, J. Zhang, T.-Q. Nguyen, G. C. Bazan and A. J. Heeger, *Nano Letters* **13:**3796-3801 (2013).
47 A. Hadipour, D. Cheyns, P. Heremans and B. P. Rand, *Advanced Energy Materials* **1:**930-935 (2011).
48 S. H. Park, A. Roy, S. Beaupre, S. Cho, N. Coates, J. S. Moon, D. Moses, M. Leclerc, K. Lee and A. J. Heeger, *Nature Photonics* **3:**297-302 (2009).
49 M. Gaceur, S. B. Dkhil, D. Duché, F. Bencheikh, J.-J. Simon, L. Escoubas, M. Mansour, A. Guerrero, G. Garcia-Belmonte, X. Liu, M. Fahlman, W. Dachraoui, A. K. Diallo, C. Videlot-Ackermann, O. Margeat and J. Ackermann, *Advanced Functional Materials* **26:**243-253 (2016).
50 J. Liu, S. Shao, B. Meng, G. Fang, Z. Xie, L. Wang and X. Li, *Applied Physics Letters* **100:**213906 (2012).
51 S. Seethamraju, P. C. Ramamurthy and G. Madras, *Physical Chemistry Chemical Physics* **17:**23165-23172 (2015).
52 V. C. Tung, J. Kim, L. J. Cote and J. Huang, *Journal of the American Chemical Society* **133:**9262-9265 (2011).
53 C.-H. M. Chuang, P. R. Brown, V. Bulović and M. G. Bawendi, *Nat Mater* **13:**796-801 (2014).
54 V. Gupta, A. K. K. Kyaw, D. H. Wang, S. Chand, G. C. Bazan and A. J. Heeger, *Sci Rep* **3:**(2013).
55 J. Bullock, P. Zheng, Q. Jeangros, M. Tosun, M. Hettick, C. M. Sutter-Fella, Y. Wan, T. Allen, D. Yan, D. Macdonald, S. De Wolf, A. Hessler-Wyser, A. Cuevas and A. Javey, *Advanced Energy Materials* **6:**n/a-n/a (2016).
56 B. Li, H. Ren, H. Yuan, A. Karim and X. Gong, *ACS Photonics* **1:**87-90 (2014).
57 A. Guerrero, S. Chambon, L. Hirsch and G. Garcia-Belmonte, *Advanced Functional Materials* **24:**6234-6240 (2014).
58 Z. Liang, Q. Zhang, L. Jiang and G. Cao, *Energy & Environmental Science* **8:**3442-3476 (2015).
59 G. Dennler, M. C. Scharber and C. J. Brabec, *Advanced Materials* **21:**1323-1338 (2009).
60 C. Duan, C. Zhong, C. Liu, F. Huang and Y. Cao, *Chemistry of Materials* **24:**1682-1689 (2012).
61 L. Zhang, C. Liu, T. Lai, H. Huang, X. Peng, F. Huang and Y. Cao, *Journal of Materials Chemistry A* **4:**15156-15161 (2016).
62 H. B. Michaelson, *Journal of Applied Physics* **48:**4729-4733 (1977).

63 S. Chen, J. R. Manders, S.-W. Tsang and F. So, *Journal of Materials Chemistry* **22:**24202-24212 (2012).
64 V. I. Madogni, B. Kounouhéwa, A. Akpo, M. Agbomahéna, S. A. Hounkpatin and C. N. Awanou, *Chemical Physics Letters* **640:**201-214 (2015).
65 Y. Zhang, W. Cui, Y. Zhu, F. Zu, L. Liao, S.-T. Lee and B. Sun, *Energy & Environmental Science* **8:**297-302 (2015).
66 S. Woo, W. Hyun Kim, H. Kim, Y. Yi, H.-K. Lyu and Y. Kim, *Advanced Energy Materials* **4:**1301692-n/a (2014).
67 B. Li, C. Zheng, H. Liu, J. Zhu, H. Zhang, D. Gao and W. Huang, *ACS Applied Materials & Interfaces* **8:**27438-27443 (2016).
68 Z. Wang, Z. Li, X. Xu, Y. Li, K. Li and Q. Peng, *Advanced Functional Materials* **26:**4643-4652 (2016).
69 S. Shao, J. Liu, J. Bergqvist, S. Shi, C. Veit, U. Würfel, Z. Xie and F. Zhang, *Advanced Energy Materials* **3:**349-355 (2013).
70 W. Zhang, X. Bi, X. Zhao, Z. Zhao, J. Zhu, S. Dai, Y. Lu and S. Yang, *Organic Electronics* **15:**3445-3451 (2014).
71 K. W. Wong, H. L. Yip, Y. Luo, K. Y. Wong, W. M. Lau, K. H. Low, H. F. Chow, Z. Q. Gao, W. L. Yeung and C. C. Chang, *Applied Physics Letters* **80:**2788-2790 (2002).
72 B. Meng, Y. Fu, Z. Xie, J. Liu and L. Wang, *Macromolecules* **47:**6246-6251 (2014).
73 K. Zhang, Z. Hu, R. Xu, X. F. Jiang, H. L. Yip, F. Huang and Y. Cao, *Advanced Materials* **27:**3607-3613 (2015).
74 C. He, C. Zhong, H. Wu, R. Yang, W. Yang, F. Huang, G. C. Bazan and Y. Cao, *Journal of Materials Chemistry* **20:**2617-2622 (2010).
75 R. Kang, S.-H. Oh and D.-Y. Kim, *ACS Applied Materials & Interfaces* **6:**6227-6236 (2014).
76 I. Osaka and R. D. McCullough, *Accounts of Chemical Research* **41:**1202-1214 (2008).
77 K. Zilberberg, A. Behrendt, M. Kraft, U. Scherf and T. Riedl, *Organic Electronics* **14:**951-957 (2013).
78 J. Kim, G. Kim, Y. Choi, J. Lee, S. H. Park and K. Lee, *Journal of Applied Physics* **111:**114511 (2011).
79 D. Zhou, X. Cheng, H. Xu, H. Yang, H. Liu, F. Wu, L. Chen and Y. Chen, *Journal of Materials Chemistry A* **4:**18478-18489 (2016).
80 U. Scherf, A. Gutacker and N. Koenen, *Accounts of Chemical Research* **41:**1086-1097 (2008).
81 Y.-H. Lin, K. A. Smith, C. N. Kempf and R. Verduzco, *Polymer Chemistry* **4:**229-232 (2013).
82 A. Gutacker, S. Adamczyk, A. Helfer, L. E. Garner, R. C. Evans, S. M. Fonseca, M. Knaapila, G. C. Bazan, H. D. Burrows and U. Scherf, *Journal of Materials Chemistry* **20:**1423-1430 (2010).
83 A. Gutacker, N. Koenen, U. Scherf, S. Adamczyk, J. o. Pina, S. M. Fonseca, A. J. M. Valente, R. C. Evans, J. Seixas de Melo, H. D. Burrows and M. Knaapila, *Polymer* **51:**1898-1903 (2010).
84 M. Knaapila, R. C. Evans, A. Gutacker, V. M. Garamus, M. Torkkeli, S. Adamczyk, M. Forster, U. Scherf and H. D. Burrows, *Langmuir* **26:**5056-5066 (2010).
85 G. Tu, H. Li, M. Forster, R. Heiderhoff, L. J. Balk, R. Sigel and U. Scherf, *Small* **3:**1001-1006 (2007).
86 H. Sirringhaus, P. J. Brown, R. H. Friend, M. M. Nielsen, K. Bechgaard, B. M. W. Langeveld-Voss, A. J. H. Spiering, R. A. J. Janssen, E. W. Meijer, P. Herwig and D. M. de Leeuw, *Nature* **401:**685-688 (1999).
87 C.-K. Mai, T. Arai, X. Liu, S. L. Fronk, G. M. Su, R. A. Segalman, M. L. Chabinyc and G. C. Bazan, *Chemical Communications* **51:**17607-17610 (2015).
88 T. Ghoos, J. r. m. Brassinne, C.-A. Fustin, J.-F. o. Gohy, M. Defour, N. Van den Brande, B. Van Mele, L. Lutsen, D. J. Vanderzande and W. Maes, *Polymer* **54:**6293-6304 (2013).
89 G. Pirotte, J. Kesters, P. Verstappen, S. Govaerts, J. Manca, L. Lutsen, D. Vanderzande and W. Maes, *ChemSusChem* **8:**3228-3233 (2015).

90 A. Garcia, J. Z. Brzezinski and T.-Q. Nguyen, *The Journal of Physical Chemistry C* **113:**2950-2954 (2009).
91 M. Kang, O. K. Nag, R. R. Nayak, S. Hwang, H. Suh and H. Y. Woo, *Macromolecules* **42:**2708-2714 (2009).
92 Z. B. Henson, Y. Zhang, T.-Q. Nguyen, J. H. Seo and G. C. Bazan, *Journal of the American Chemical Society* **135:**4163-4166 (2013).
93 D. Tordera, M. Kuik, Z. D. Rengert, E. Bandiello, H. J. Bolink, G. C. Bazan and T.-Q. Nguyen, *Journal of the American Chemical Society* **136:**8500-8503 (2014).
94 R. Yang, A. Garcia, D. Korystov, A. Mikhailovsky, G. C. Bazan and T.-Q. Nguyen, *Journal of the American Chemical Society* **128:**16532-16539 (2006).
95 A. Thomas, J. E. Houston, N. Van den Brande, J. De Winter, M. Chevrier, R. K. Heenan, A. E. Terry, S. Richeter, A. Mehdi, B. Van Mele, P. Dubois, R. Lazzaroni, P. Gerbaux, R. C. Evans and S. Clement, *Polymer Chemistry* **5:**3352-3362 (2014).
96 L. Chen, C. Xie and Y. Chen, *Macromolecules* **47:**1623-1632 (2014).
97 Y. Yuan, P. Sharma, Z. Xiao, S. Poddar, A. Gruverman, S. Ducharme and J. Huang, *Energy & Environmental Science* **5:**8558-8563 (2012).
98 M. J. Stephen and J. P. Straley, *Reviews of Modern Physics* **46:**617-704 (1974).
99 B. F. De Oliveira, P. P. Avelino, F. Moraes and J. C. R. E. Oliveira, *Physical Review E* **82:**041707 (2010).
100 J. Fang, B. H. Wallikewitz, F. Gao, G. Tu, C. Müller, G. Pace, R. H. Friend and W. T. S. Huck, *Journal of the American Chemical Society* **133:**683-685 (2011).
101 C. Hoven, R. Yang, A. Garcia, A. J. Heeger, T.-Q. Nguyen and G. C. Bazan, *Journal of the American Chemical Society* **129:**10976-10977 (2007).
102 C. Duan, L. Wang, K. Zhang, X. Guan and F. Huang, *Advanced Materials* **23:**1665-1669 (2011).
103 Y. Liu, V. V. Duzhko, Z. A. Page, T. Emrick and T. P. Russell, *Accounts of Chemical Research* **49:**2478-2488 (2016).
104 Z. A. Page, V. V. Duzhko and T. Emrick, *Macromolecules* **46:**344-351 (2013).
105 F. Liu, Z. A. Page, V. V. Duzhko, T. P. Russell and T. Emrick, *Advanced Materials* **25:**6868-6873 (2013).
106 Z. A. Page, F. Liu, T. P. Russell and T. Emrick, *Journal of Polymer Science Part A: Polymer Chemistry* **53:**327-336 (2015).
107 Y. Liu, Z. A. Page, T. P. Russell and T. Emrick, *Angewandte Chemie International Edition* **54:**11485-11489 (2015).
108 Y. Cao, G. Yu, C. Zhang, R. Menon and A. J. Heeger, *Synthetic Metals* **87:**171-174 (1997).
109 M. P. d. Jong, L. J. v. IJzendoorn and M. J. A. d. Voigt, *Applied Physics Letters* **77:**2255-2257 (2000).
110 K. Norrman, N. B. Larsen and F. C. Krebs, *Solar Energy Materials and Solar Cells* **90:**2793-2814 (2006).
111 B. J. Worfolk, T. C. Hauger, K. D. Harris, D. A. Rider, J. A. M. Fordyce, S. Beaupré, M. Leclerc and J. M. Buriak, *Advanced Energy Materials* **2:**361-368 (2012).
112 M. Carrara, J. J. Kakkassery, J.-P. Abid and D. J. Fermín, *ChemPhysChem* **5:**571-575 (2004).
113 E. J. Lee, J. P. Han, S. E. Jung, M. H. Choi and D. K. Moon, *ACS Applied Materials & Interfaces* **8:**31791-31798 (2016).
114 B. H. Lee, J.-H. Lee, S. Y. Jeong, S. B. Park, S. H. Lee and K. C. Lee, *Advanced Energy Materials* **5:**1401653-n/a (2015).
115 J.-H. Lee, B. H. Lee, S. Y. Jeong, S. B. Park, G. Kim, S. H. Lee and K. C. Lee, *Advanced Energy Materials* **5:**1501292-n/a (2015).
116 C. Xie, L. Chen and Y. Chen, *J Phys Chem C* **117:**24804-24814 (2013).
117 T. Yang, M. Wang, C. Duan, X. Hu, L. Huang, J. Peng, F. Huang and X. Gong, *Energy & Environmental Science* **5:**8208-8214 (2012).
118 H. Choi, J. S. Park, E. Jeong, G.-H. Kim, B. R. Lee, S. O. Kim, M. H. Song, H. Y. Woo and J. Y. Kim, *Advanced Materials* **23:**2759-2763 (2011).
119 W. S. Yang, J. H. Noh, N. J. Jeon, Y. C. Kim, S. Ryu, S. J. and S. Il Seok, *Science* **348:**1234-1237 (2015).

120 S. D. Stranks, G. E. Eperon, G. Grancini, C. Menelaou, M. J. P. Alcocer, T. Leijtens, L. M. Herz, A. Petrozza and H. J. Snaith, *Science* **342:**341-344 (2013).
121 J. Burschka, N. Pellet, S.-J. Moon, R. Humphrey-Baker, P. Gao, M. K. Nazeeruddin and M. Grätzel, *Nature* **499:**316-319 (2013).
122 H. Kim, K.-G. Lim and T.-W. Lee, *Energy & Environmental Science* **9:**12-30 (2016).
123 Q. Lin, A. Armin, R. C. R. Nagiri, P. L. Burn and P. Meredith, *Nature Photonics* **9:**106-102 (2015).
124 H. Zhang, H. Azimi, Y. Hou, T. Ameri, T. Przybilla, E. Spiecker, M. Kraft, U. Scherf and C. J. Brabec, *Chemistry of Materials* **26:**5190-5193 (2014).